Slow fluctuation of Rac1 activity is associated with biological and transcriptional heterogeneity of glioma cells(Dissertation_全文)

AUTHOR(S):

Yukinaga, Hiroko

Research Article

Slow fluctuation of Rac1 activity is associated with biological and transcriptional heterogeneity of glioma cells

H. Yukinaga[1], C. Shionyu[2], E. Hirata[2], K. Ui-Tei[3], T. Nagashima[4,6], S. Kondo[4], M. Okada-Hatakeyama[5], H. Naoki[7], M. Matsuda[1,2,8]*

[1]Department of Pathology and Biology of Diseases, Graduate School of Medicine, Kyoto University, Kyoto, Japan, [2]Laboratory of Bioimaging and Cell Signaling, Graduate School of Biostudies, Kyoto University, Kyoto, Japan, [3]Department of Biophysics and Biochemistry, Graduate School of Science, University of Tokyo, Tokyo, Japan, [4]Research Unit for Immunodynamics, RIKEN Research Center for Allergy and Immunology, Yokohama, Japan, [5]Laboratory for Cellular Systems Modeling, RIKEN Research Center for Allergy and Immunology, Yokohama, Japan, [6]Division of Cell Proliferation, United Centers for Advanced Research and Translational Medicine, Tohoku University Graduate School of Medicine, [7]Imaging Platform for Spatio-Temporal Information, Graduate School of Medicine, Kyoto University, [8]Institute for Integrated Cell-Material Sciences, Kyoto University, Japan.

*To whom correspondence should be addressed.

Mailing address: Department of Pathology and Biology of Diseases, Graduate School of Medicine, Kyoto University, Kyoto, Yoshida-Konoe-Cho, Sakyo-ku, Kyoto 606-8501, Kyoto, Japan

Tel: 81-75-753-4421

FAX: 81-75-753-4655

E-mail: matsuda.michiyuki.2c@kyoto-u.ac.jp

Running title: Heterogeneity by fluctuation of Rac1 activity

Keywords: Rac1/Invasion/Heterogeneity/

Summary

Phenotypic heterogeneity of cancer cells is caused not only by genetic and epigenetic alterations, but also by stochastic variation of intracellular signaling molecules. Using cells that stably express Förster resonance energy transfer (FRET) biosensors, we here show correlation of Rac1 activity fluctuation with invasive property of C6 glioma cells. By long-term time-lapse imaging Rac1 activity in C6 glioma cells was found to fluctuate with a timescale significantly longer than the replication cycle. Because the level of Rac1 activity in each cell was robust to suspension-adhesion procedure, C6 glioma cells were sorted by Rac1 activity, yielding $Rac1^{high}$ and $Rac1^{low}$ cells. The $Rac1^{high}$ cells invaded more efficiently than did $Rac1^{low}$ cells in the Matrigel invasion assay. Among the top 14 membrane-related genes enriched in $Rac1^{high}$ cells, four genes were associated with glioma invasion and Rac1 activity as examined by siRNA knockdown experiments. Among transcription factors enriched in $Rac1^{high}$ cells, Egr2 was found to positively regulate expression of the four membrane-related invasion-associated genes. The identified signaling network may cause the slow fluctuation of Rac1 activity and heterogeneity in invading capacity of glioma cells.

Introduction

Cancer cells originated from a single cell acquire phenotypic heterogeneity due to genomic instability or heritable epigenetic changes (Lengauer et al., 1998; Shackleton et al., 2009). This heterogeneity is of great advantage for the cancer progression and guarantees its insidious, highly invasive nature in tissues (Heppner, 1984; Rubin, 1990; Shackleton et al., 2009). Recently, however, it has also been reported that the fate and behavior of mammalian cells, including cancer cells, can be determined by stochastic gene expression variation (Brock et al., 2009). For example, patterns of signaling heterogeneity in monoclonal cancer cells can generate diverse phenotypes with different drug sensitivities (Singh et al., 2010).

A typical example of cancers that exhibit extensive heterogeneity is glioblastoma, which was previously termed glioblastoma "multiforme," reflecting its histopathological divergence in size, shape, karyotype, etc. (Louis, 2006). Among the many experimental models of glioblastoma, the C6 glioma cell model has been frequently used to study invasiveness of glioblastoma cells (Grobben et al., 2002). The C6 glioma cells implanted into syngeneic Wistar rats share many histological hallmarks with human glioblastoma and preferentially migrate along neuronal fibers and through the perivascular space, a pattern which resembles the spread of human glioblastoma.

Rho-family GTPases regulate cytoskeletal dynamics and thereby affect many cellular processes, including cell polarity, migration, vesicle trafficking and cytokinesis (Etienne-Manneville and Hall, 2002). In cancer cells, Rho-family GTPases play critical roles in manifesting the cancer cell-specific behavior (Sahai and Marshall, 2002). Rac1, for

example, accelerates tumorigenesis by regulating apoptosis, cell cycle progression, assembly and disassembly of tight junction and adherens junction, cell migration, and cell invasion (Mack et al., 2011). Importantly, these pleiotropic functions of Rho-family GTPases have been characterized by comparing cancer cells with non-cancer cells. Meanwhile, little is known about the heterogeneity and fluctuation of Rho-family GTPase activity within the cancer cell population.

Sorting cells with respect to a property of interest is essential to study the heterogeneity of cancer cells by genetic, epigenetic, biochemical, or cell biological analyses. Cell surface markers and cognitive antibodies have been routinely used for this purpose, but the methods used to sort cells depending on the intracellular activity of a signaling molecule are limited. Biosensors based on the principle of Förster resonance energy transfer (FRET) have been widely used to monitor the activity of the signaling molecules (Kiyokawa et al., 2006; Miyawaki, 2011); however, due to a lack of methods for the stable expression of the FRET biosensors, cell sorting with FRET biosensor-expressing cells has been a difficult task.

Recently, we developed methods to express FRET biosensors stably in cell lines and transgenic mice (Kamioka et al., 2012; Komatsu et al., 2011). With C6 rat glioma cells stably expressing a FRET biosensor for Rac1, we found that C6 glioma cells penetrating the brain parenchyma showed higher Rac1 and Cdc42 activities and lower RhoA activity than those advancing in the perivascular regions (Hirata et al., 2012). This observation urged us to investigate the mechanism by which the heterogeneity of Rho-family GTPase activity is generated, and the role of the heterogeneity in the invasion of glioma cells. For this purpose, we established a method to sort cells with respect to their levels of Rho-family GTPase activity. Then, by using next-generation sequencers, we identified genes whose expressions were correlated with Rac1 activity. Using this approach, we here show that slow fluctuation of Rac1 activity is associated with the heterogeneity of glioma invasion.

Results

Distribution of Rac1 activity among C6 glioma cells

We have shown that C6 glioma cells invading at the periphery of a tumor mass in the rat brain or a 3D spheroid exhibit higher Rac1 activity than those trailing such leader cells (Hirata et al., 2012). We speculated that such distribution of Rac1 activity among C6 glioma cells may be autonomously generated during cell growth and spreading. To test this idea, we prepared C6 glioma cells that stably express a FRET biosensor, Raichu-Rac1, and visualized Rac1 activity on glass-bottom dishes (Fig. 1A). We detected significant variation in Rac1

activity, which exhibited a typical normal distribution (Fig. 1B, C). Correlation between the Rac1 activity and the expression level of the biosensor was not observed (Fig. 1D)

Fluctuation and Robustness of Rac1 activity

The normal distribution of Rac1 activity probably reflected the noise of the system (Brock et al., 2009). To study the mechanism underlying the generation of the noise, we time-lapse imaged Rac1 activity in C6 glioma cells for 5 days (Fig. 2A, Movie S1). C6 glioma cells expressing Raichu-Rac1 were seeded onto a glass-bottom dish having 282-μm-diameter spot, which prevented cells from straying out from the visual field. To maintain cell density within the optimal range for cell growth, the Raichu-Rac1-expressing cells were co-cultured with parental C6 glioma cells. We chose spots having a single biosensor-expressing cell and one to several parental C6 cells for the tracking. Rac1 activity was averaged over the entire cell area and plotted against time (Fig. 2B). Except for the rapid decline and increment during cell division, Rac1 activity exhibited fluctuation with timescales longer than the cell cycle (>40 hours). Consequently, after 5 days, when the single cells proliferated to 6 to 8 cells, Rac1 activity varied significantly among the daughter cells (Supplementary Fig. S1A). Analysis with power spectrum did not reveal any periodicity of Rac1 activity fluctuation (Fig. 2C). Of note, Rac1 activity did not significantly change before and after cell division, suggesting that the level of Rac1 activity was maintained by a mechanism that is robust to cell division (Fig. 2D). The range of Rac1 activity after 5 days (Fig. 2B) was similar to the range of Rac1 activity observed for the cell population (Fig. 1C). Therefore, we concluded that the distribution of Rac1 activity was generated primarily by the slow fluctuation with timescales longer than the cell cycle. To understand the biological significance of the observed distribution of Rac1 activity, we examined the correlation between the cell area and Rac1 activity (Fig. 2E), and found a weak positive correlation. The positive, albeit weak, correlation between cell area and Rac1 activity probably reflects the high level of Rac1 activity in lamellipodia (Itoh et al., 2002; Kraynov et al., 2000). We also examined the velocity of migration (Fig. 2E), but could not observe any clear correlation with Rac1 activity.

Next, to examine the robustness of the level of Rac1 activity, we detached the cells by trypsin, and then induced cell adhesion by trypsin inhibition in situ (Fig. 2F). Trypsinization induced cell rounding and decreased Rac1 activity. Following trypsin inhibition induced cell adhesion and restored the Rac1 activity. Notably, the relative Rac1 activity of each cell did not change before, during, and after trypsinization (Fig. 2F). This observation agrees with the previous report that the suspension of adherent cells reduces Rac1 activity (del Pozo et al., 2000), and also suggests that the level of Rac1 activity in

each cell is maintained by a robust mechanism, which is not affected by the suspension-adhesion procedure.

FRET-based cell sorting to select Rac1^{high} and Rac1^{low} populations

To understand the mechanisms underlying and roles played by the slow fluctuation and robustness of Rac1 activity, we attempted to examine the transcriptomes of C6 glioma cells with different levels of Rac1 activity. Encouraged by the observation that the suspension-adhesion procedure did not alter the relative Rac1 activity of each cell, we sorted C6 glioma cells depending on Rac1 activity with FACS. The FRET/CFP ratio was used as the index of FRET efficiency as in microscopy. The FRET/CFP ratio was independent of the expression level of the biosensor (Fig. 3A) as observed in 2D condition (Fig. 1D). C6 glioma cells in the highest and lowest decile with respect to the FRET/CFP ratio were named the Rac1^{high} and Rac1^{low} populations, respectively, and sorted (Fig. 3B).

There was a serious concern about whether the Rac1 activity monitored by the FRET/CFP ratio in FACS reflected the Rac1 activity of cells grown on the culture dishes, because Rac1 activity is closely associated with cell attachment (del Pozo et al., 2000). In Fig. 2F, we showed that suspension-adhesion procedure did not alter the relative Rac1 activity of each cell among the cell population. Here, we quantified GTP bound to the endogenous Rac1 by pulldown assay. The amount of GTP-Rac1 in Rac1^{high} cells was larger than that in Rac1^{low} cells (Fig. 3C). Furthermore, we directly measured the GTP/GDP ratio by TLC after cell sorting. Both Rac1^{high} and Rac1^{low} cells were plated on the culture dishes and labeled with $^{32}P_i$ for 2 hours, followed by TLC analysis to measure the GTP/GDP ratio on the biosensor (Fig. 3D). Although the difference in the GTP/GDP ratio between Rac1^{high} and Rac1^{low} was smaller than the difference between wild-type and GTPase-deficient mutant Rac1 proteins, the GTP/GDP ratio of Rac1^{high} cells was constantly higher than that of Rac1^{low} cells, providing a biochemical validation of the FRET-based cell sorting. In addition, we found that cells in G2/M phases were enriched in Rac1^{low} cell (Supplementary Fig. S1B), which agrees with the observation that Rac1 activity transiently dropped during cell division (Fig. 2B).

We then examined the invasion of Rac1^{high} and Rac1^{low} cells into Matrigel by Boyden chamber assay. Cells that had reached the lower side of filter were counted after 22 hours. Although the efficiency of invasion varied in each experiment, we constantly observed that Rac1^{high} cells invaded into Matrigel significantly faster than did Rac1^{low} cells (Fig. 3E). This observation agrees with the findings of our previous 3D spheroid assay that cells with higher Rac1 activity invaded into Matrigel at the front and guided cells with lower Rac1 activity (Fig. 1B) (Hirata et al., 2012).

Finally, to confirm our hypothesis that the distribution of Rac1 activity was caused by slow fluctuations, the $Rac1^{high}$ and $Rac1^{low}$ cells were cultured for up to nine days and re-analyzed by FACS. On the first day, the distribution of Rac1 activities within the sorted populations remained discrete, but after one week the distribution of Rac1 activity within each population was identical, supporting our hypothesis (Fig. 3F). We performed similar experiments with C6 glioma cells expressing a FRET biosensor for Cdc42. In agreement with the previous finding that the glioma cells invading at the front exhibit high Rac1 activity and high Cdc42 activity (Hirata et al., 2012), a similar result was obtained with $Cdc42^{high}$ and $Cdc42^{low}$ cells (Fig. 3F). Furthermore, we retrogradely analyzed long-term time-lapse images (Supplementary Fig. S1C), and found that, in agreement with the FACS data, cells in the highest and lowest decile with respect to the FRET/CFP ratio were merging in fifty hours.

Transcriptional signatures of $Rac1^{high}$ and $Rac1^{low}$ cells

To investigate the association of the Rac1 activity variation with transcriptional signatures, RNA-Seq analysis was performed with C6 glioma cells sorted by FACS. mRNA was isolated from the $Rac1^{high}$ and $Rac1^{low}$ populations of C6 glioma cells and sequenced. The expression difference of $Rac1^{high}$/$Rac1^{low}$ was plotted against average expression (Fig. 4A). Similar analysis was performed for Cdc42 and RhoA to characterize the nature of the $Rac1^{high}$ and $Rac1^{low}$ populations (Fig. 4B). The difference in the expression of $Rac1^{high}$/$Rac1^{low}$ was positively correlated with that of $Cdc42^{high}$/$Cdc42^{low}$. But there was no correlation between the expression differences of $Rac1^{high}$/$Rac1^{low}$ and $RhoA^{high}$/$RhoA^{low}$ or those of $Cdc42^{high}$/$Cdc42^{low}$ and $RhoA^{high}$/$RhoA^{low}$. Again, this is in agreement with our previous observation that both Rac1 and Cdc42 activities were high in cells migrating at the front of glioma cells in rat brains and in 3D Matrigel (Hirata et al., 2012). For identification of differentially expressed genes, we used the weighted average difference method (WAD). The WAD method identified 713 differentially expressed genes using a cutoff of the top 5% of ranked genes. Gene ontology analysis based on biological process terms showed that the $Rac1^{high}$ phenotype is associated with the GPCR protein signaling pathway, cell-matrix adhesion, and electron transport chain in that order (Fig. 4C). The $Rac1^{low}$ phenotype is associated with cell division, cell cycle, and mitosis terms. In addition, analysis with cellular component terms showed that genes related to the respiratory chain, focal adhesion, and mitochondrial respiratory chain complex I, were enriched in the $Rac1^{high}$ population, and that genes related to the cytoplasm, nucleus, and integral to membrane were enriched in $Rac1^{low}$ population (Fig. 4D).

Identification of genes that regulate C6 glioma cell invasion

Based on the RNA-Seq data, we attempted to identify genes that regulate glioma invasion. For this purpose, we focused on the top 23 up-regulated genes related to cell component term "membrane" (Table S1). Notably, 18 genes out of the 23 genes were up-regulated in $Cdc42^{high}$ cells in comparison to $Cdc42^{low}$ cells, strongly suggesting that a large part of $Rac1^{high}$ cells are overlapped with $Cdc42^{high}$ cells. Before starting detailed characterization of the membrane-related genes enriched in $Rac1^{high}$ cells, the difference in gene expression between $Rac1^{high}$ cells and $Rac1^{low}$ cells was confirmed by qPCR, except for Ecop, to which we failed to prepare specific primers. Next, we knocked-down top 10 genes with three different siRNAs, except for cathepsin L1 (ctsl1), against which we failed to prepare three effective siRNAs. From the remaining 12 genes, we arbitrarily chose and knocked-down Ntrk2, Freq, Il1rap, and Pstpip2. C6 glioma cells were then examined for their invasive potential by the Matrigel invasion assay. Among the 14 membrane-related genes, knockdown of MMP15, TSN17, Pstpip2, and Freq, which we call membrane-related invasion-associated genes, significantly inhibited C6 glioma cell invasion (Fig. 5A). Except for MMP15, knockdown of the membrane-related invasion-associated genes suppressed Rac1 activity, suggesting thatTSN17, Pstpip2, and Freq promoted invasion via Rac1 activation (Fig. 5B). Knockdown of membrane-related but invasion-irrelevant genes, Lgals3 and Rgs2, did not affect Rac1 activity. Notably, knockdown of TSN17 and Freq, but not Pstpip2, caused rounding of the cell shape (Fig. 5C). These two genes may be associated with Rac1-mediated membrane protrusion.

We next sought for transcription factors enriched in $Rac1^{high}$ cells (Table S2), and found that Egr2 was reproducibly enriched in $Rac1^{high}$ cells and $Cdc42^{high}$ cells. Similarly, we identified Elmo1 and PRex1 as Rac1 activators enriched in $Rac1^{high}$ cells (Table S3). Knockdown of Egr2 and Elmo1, but not PRex1, suppressed C6 cell invasion and decreased Rac1 activity (Fig. 5D, E). Unlike the knockdown of membrane-related genes, TSN17 and Freq, knockdown of Egr2 or Elmo1 decreased Rac1 activity without affecting the cell shape (Fig. 5F).

Thus, we identified genes of four membrane-related proteins, a transcriptional factor, and a Rac1 activator as invasion-associated genes enriched in $Rac1^{high}$ cells. Notably, knockdown of Egr2, Elmo1, Pstpip2, Freq, and TSN17 not only decreased the average Rac1 activity but also suppressed the fluctuation of Rac1 activity (Supplementary Fig. S2), implying that the fluctuation of Rac1 activity may be associated with the basal level of Rac1 activity.

Hierarchy of the invasion-associated genes enriched in $Rac1^{high}$ cells

To untangle the signaling network of the invasion-associated genes enriched in $Rac1^{high}$ cells, we first transiently activated Rac1 by rapamycin-induced Rac1 activation system

(Yagi et al., 2012). Upon rapamycin-induced membrane translocation of Tiam1, a GEF for Rac1, Rac1 activation was clearly detected by both FACS (Fig. 6A) and pulldown assay (Fig. 6B). Among the genes tested, only Egr2 was significantly induced rapidly and transiently (Supplementary Fig. S3). We next knocked down each gene and quantified the expression of the other invasion-associated genes by qPCR (Supplementary Fig. S4). The comprehensive knockdown experiments revealed intriguing features of the signaling network that regulates Rac1 activity (Fig. 6C). First, the membrane-related invasion-associated genes, Pstpip2, TSN17, Freq, and MMP15, could be clustered by the response to the knockdown of the other genes. Second and more importantly, we could infer the hierarchy of the genes by assuming that the knockdown of a gene decreases the expression of the downstream genes and increases the expression of the upstream gene(s) by a negative feedback loop. For example, Egr2 knockdown decreased expression of all four membrane-related invasion-associated genes, but not an invasion-irrelevant gene, Rgs2, or Elmo1. On the other hand, knockdown of the membrane-related invasion-associated genes increased Egr2 expression, suggesting the presence of negative feedback loops to Egr2. Because the effect of Egr2 knockdown on the expression of Pstpip2 was not significant, this gene may be placed in a different signaling pathway. From these data, we suggest a model of the gene network that regulates Rac1 activity and invasion of C6 glioma cells (Fig. 6D).

Discussion

The phenotypic heterogeneity of cancer cell populations is caused by genetic, epigenetic, and non-genetic mechanisms. The non-genetic mechanism that causes the variation of gene expression includes transcriptional and translational noises (Brock et al., 2009). Although the precise nature of such noise remains largely elusive, we can speculate that the gene expression variation would reflect the intracellular signaling activities. Here we established a technology to sort the cells depending on the activities of intracellular signaling molecules and to examine the effect of the activity variation of signaling molecules on the biological or transcriptional heterogeneity of cancer cells.

FRET-based cell sorting

The technology is based on two assumptions. First, the activity of the molecule of interest is maintained during FACS. Second, the transcriptome is not significantly perturbed during FACS. We had a serious concern as to whether the process of cell preparation, i.e., trypsinization and suspension of adherent C6 glioma cells, might mask the intercellular variation in the activities of Rho-family GTPases that are observed both under 2D and 3D

conditions. In fact, it has been established that the suspension of adherent cells reduces their Rac1 activity (del Pozo et al., 2000). Contrary to our expectation, however, the intercellular variation in Rac1 activity was reproduced after the cell preparation. Reanalysis of Rac1 activity by FACS, TLC, or pulldown assay demonstrated that Rac1 activity was conserved in both the $Rac1^{high}$ and $Rac1^{low}$ cell populations (Fig. 3A, B). Time-lapse imaging confirmed that the relative Rac1 activity of each cell was maintained before and after cell division or suspension-adhesion procedure (Fig. 2D). These observations imply that the Rac1 activity in a single cell consists of basal and external cue-dependent Rac1 activities. The external cue includes integrin, growth factors, etc., and rapidly changes Rac1 activity upon input of the cues (Heasman and Ridley, 2008). Meanwhile, the basal Rac1 activity is determined by intrinsic signaling status, which is robust to external cues and is subjected to fluctuation with longer timescales.

The second assumption that needs further consideration is the effect of cell sorting on the transcriptome. The ontology analysis of genes enriched in $Rac1^{high}$ cells showed close correlation to biological process terms that are linked to the function of Rac1 (Fig. 4C). The first and second scores went to the GPCR pathway and cell-matrix adhesion. Both of these are related to cell migration, with which the functions of Rac1 are most often associated (Sahai and Marshall, 2002; Sander and Collard, 1999). Another major function of Rac1 is the regulation of NADH-mediated production of reactive oxygen species (Heasman and Ridley, 2008); therefore, it is not surprising that the electron transport chain was scored at the third position. Furthermore, in agreement with the finding that Rac1 activity drops rapidly during cell division (Yoshizaki et al., 2003), the first to third scores of genes enriched in $Rac1^{low}$ cells went to the pathways of cell division, cell cycle, and mitosis (Fig. 4C). Furthermore, among the 23 genes up-regulated in the $Rac1^{high}$ population and classified under the cell component term “membrane”, 13 genes are known to be involved in cancer cell invasion (Table S1). These observations support our assumption that the transcriptional profiles are reasonably conserved during FACS.

Genes associated with the $Rac1^{high}$ phenotype

Among the 14 genes classified under the cell component term “membrane” and enriched in $Rac1^{high}$ cells, knockdown of 4 genes inhibited C6 glioma cell invasion in the Matrigel invasion assay. Previous reports have indicated or suggested that proteins encoded by the four genes are more or less associated with invasion of cancer cells. MMP15, matrix metaloprotease protein 15 of MT2-MMP, is expressed predominantly in glioblastoma (Lampert et al., 1998; Nakada et al., 1999), suggesting that MMP15 may play a major role in the degradation of extracellular matrix during glioma invasion. TSN17, tetraspanin 17, was recently shown to regulate ADAM10, which has been shown to be involved in cancer

progression (Dornier et al., 2012; Haining et al., 2012; Mochizuki and Okada, 2007). Pstpip2 regulates F-actin bundling and enhances filopodia (Chitu et al., 2005), which strongly argues for a role of this protein in glioma invasion. Freq is a calcium-binding protein expressed predominantly in neuronal cells (Dason et al., 2012; Nakamura et al., 2006). In primary cultured adult cortical neurons, overexpression of NCS1 induces neurite sprouting; however, the role of NCS-1 in glioma invasion has not been determined.

Genes responsive to the activation of Rac1 or Cdc42 have been identified by overexpressing constitutively active QL mutants of Rac1 or Cdc42 in NIH 3T3 cells (Teramoto et al., 2003). There are some similarities between this previous work and our present study. First, the expression profile of Rac1QL-expressing cells resembles that of Cdc42QL-expressing cells in the previous studies. We also found that the expression profile of $Rac1^{high}$ cells resembles that of $Cdc42^{high}$ cells (Fig. 4B, Table S1). Second, in cells expressing Rac1QL or Cdc42QL, genes related to the extracellular matrix and cell adhesion are enriched and genes related to the cell cycle are suppressed as in $Rac1^{high}$ cells (Fig. 4C). However, there are also some discrepancies. For example, collagen alpha 1 chain precursor was 3.1-fold enriched in Rac1QL-expressing cells, but was 0.56-fold suppressed in $Rac1^{high}$ cells. This difference may have been caused by the lack of GTPase activity in Rac1QL mutant, because the cycling between the GDP-bound and GTP-bound forms has been shown to play an important role in cell migration (Parrini et al., 2011). In another study, different levels of Rac1 were expressed in colorectal cancer cells to identify the target genes of Rac1 by microarray analysis (Gomez et al., 2007). However, we could not find any similarity to our data. In another study, C6 rat glioma cells were selected both in vitro and in vivo for high and low migratory phenotypes (Tatenhorst et al., 2005). By microarray analysis, thirty-one genes were found to be differentially expressed in association with migratory phenotypes. We could not detect a significant resemblance between the gene expression profiles of this study and our present findings. Thus, the constitutive activation (or suppression) and intrinsic fluctuation of Rac1 activity might cause different transcriptional phenotypes. Alternatively, the effect of Rac1 on transcriptional profiles might be cell-type specific. In any event, different approaches led to the identification of various genes related to glioma invasion. Further analyses will be required to find the cause of such divergence.

Hierarchy of invasion-associated genes enriched in $Rac1^{high}$ population

The comprehensive knockdown experiments strongly argued for the role of Egr2 as a master regulator of C6 glioma invasion. Knockdown of Egr2 suppressed the expression of the four membrane-related invasion-associated genes. In contrast, knockdown of the four membrane-related invasion-associated genes or Elmo1 increased the expression of Egr2,

implying negative feedback loops from the invasion phenotype to Egr2 expression. Microarray analyses have revealed enrichment of Egr2 in metastatic squamous cell carcinomas (Kim et al., 2006; Liu et al., 2008). Furthermore, in fibroblasts infected with Kaposi sarcoma-associated herpesvirus, Egr2 induces MMPs and Extracellular Matrix MetalloPRoteinase INducer (emmprin) (Dai et al., 2012). These observations strongly argue for the proposal that Egr2 is a key regulator of glioma invasion.

Origin of the heterogeneity of Rac1 activity

What causes the heterogeneity of Rac1 activity among C6 glioma cells? The five-day time-lapse image revealed that the distribution of Rac1 activity was caused by non-genetic slow fluctuation with time scales of more than 40 hours (Fig. 2A). This conclusion was also supported by the observation that the isolated $Rac1^{high}$ or $Rac1^{low}$ cell population restored the original distribution within one week (Fig. 3F, Supplementary Fig. S1C). Notably, our conclusion agrees with the variation of protein levels in human H1299 lung carcinoma cells (Sigal et al., 2006), in which the expression levels of proteins have been shown to fluctuate with a timescale of more than 40 hours. By the knockdown experiments against genes enriched in $Rac1^{high}$ population, we identified a gene network regulating Rac1 activity (Fig. 6D). This network comprises both positive and negative feedback loops, which are sufficient to cause oscillation of a signaling network. Although we have not been able to confirm that the variation in Rac1 activity in vivo is also driven by the same mechanism, slow fluctuations of gene expression, and resulting fluctuation of Rac1 activity could generate glioma cells with different levels of invading capacity.

Materials and Methods

Biosensors and cell lines

C6 rat glioma cells were obtained from American Type Culture Collection and cultured in DMEM containing 10% FBS. The FRET biosensors for Rac1, Cdc42, and RhoA, Raichu-Rac1, Raichu-Cdc42, and Raichu-RhoA, respectively, were described previously (Itoh et al., 2002; Yoshizaki et al., 2003). For the establishment of stable cell lines expressing Raichu biosensors, we took two approaches. First, we replaced CFP with teal fluorescent protein (TFP) and delivered the expression cassettes by a retroviral vector into C6 glioma cells as described previously (Hirata et al., 2012). More recently, piggyBac transposon-mediated gene transfer was used to stably express Raichu biosensors with higher sensitivity (Komatsu et al., 2011; Yusa et al., 2009) . The cells were single-cell cloned before further experiments unless described otherwise.

Time-lapse FRET imaging

FRET images were obtained and processed using essentially the same conditions and procedures as previously reported (Aoki and Matsuda, 2009). Cells were plated on 35 mm-diameter glass-bottom dishes (AGC Techno Glass, Shizuoka, Japan) or micro-patterned glass-bottom dishes (CytoGraph; Dai Nippon Printing Co., Tokyo, Japan). Cells were imaged at 37^{o}C in 5% CO_2 with an inverted microscope (IX81; Olympus, Tokyo, Japan) equipped with a x40 objective lens (UAPO/NA 1.35; Olympus), a x40 objective lens (UPLSAPO/NA 0.95; Olympus), and a x60 objective lens (PlanApoPH/NA 1.40; Olympus), a cooled CCD camera (Cool SNAP-HQ or Cool SNAP-K4; Roper Scientific, Tucson, AZ), an LED illumination system (CoolLED precisExcite; Molecular Devices, Sunnyvale, CA), an IX2-ZDC laser-based autofocusing system (Olympus) and an MD-XY30100T-Meta automatically programmable XY stage (SIGMA KOKI, Tokyo, Japan). The following filters used for the dual emission imaging studies were obtained from Omega Optical (Brattleboro, VT): an XF1071 (440AF21) excitation filter, an XF2034 (455DRLP) dichroic mirror, and two emission filters, XF3075 (480AF30) for CFP and XF3079 (535AF26) for yellow fluorescent protein (YFP). After background subtraction, FRET/CFP ratio images were created with MetaMorph software (Universal Imaging, West Chester, PA), and represented by intensity-modulated display mode. In the intensity-modulated display mode, eight colors from red to blue are used to represent the FRET/CFP ratio, with the intensity of each color indicating the mean intensity of FRET and CFP. For the quantification, the FRET and CFP intensities were averaged over the whole cell area, and the results were exported to Excel software (Microsoft Corporation, Redmond, WA).

FRET-based Cell Sorting

C6 glioma cells expressing Raichu-Rac1 were trypsinized, resuspended in PBS containing 3% FBS, and analyzed and/or sorted with a FACSAria (Becton Dickinson, Franklin Lakes, NJ). We used the following combinations of lasers and emission filters for the detection of fluorescence from the biosensor: for the donor fluorescence of TFP and CFP, a 407 nm laser and a 480AF30 filter (Omega Optical); for the sensitized FRET from YFP, a 407 nm laser and a 535AF26 filter (Omega Optical); and for the acceptor fluorescence of YFP, a 475 nm laser and a 535AF26 filter (Omega Optical). Cells were first gated for size and granularity to exclude cell debris and aggregates. For cell sorting, C6 glioma cells in the highest and lowest decile with respect to the FRET/CFP (or TFP) ratios were sorted as $Rac1^{high}$ and $Rac1^{low}$ populations, respectively, into DMEM containing 10% FBS. Small fractions of $Rac1^{high}$ and $Rac1^{low}$ were reanalyzed for validation and the remaining cells were snap-frozen and stored at -80°C until RNA extraction. Detailed data analysis was performed using FlowJo. 7.6 software (Tree Star Inc., Ashland, OR).

TLC of guanine nucleotides bound to GTPases

Guanine nucleotides bound to Raichu biosensors or GFP-tagged Rac1 proteins were quantified essentially as described previously (Gotoh et al., 1995). Briefly, cells were sorted by FACS and plated on 6-well dishes. After 3 hours, cells were metabolically labeled with $^{32}P_i$ for 2 hours and lysed with lysis buffer. The cell lysates were clarified by centrifugation and used to immunoprecipitate Raichu biosensors or GFP-tagged Rac1 with an anti-GFP antiserum and Protein-A Sepharose. Guanine nucleotides bound to the immuoprecipitates were separated by TLC and quantitated with a BAS-1000 image analyzer.

Rac1 pulldown analysis

Rac1 pulldown assay was performed according to the manufacturer's protocol (Cytoskelton, Inc, Denver, CO).

RNA extraction

Total RNA was isolated with a Qiagen RNeasy Micro Kit (Qiagen, Hilden, Germany) or a Qiagen RNeasy Mini Kit, according to the manufacturer's protocol. RNA preparations were confirmed to be free of proteins using a NanoDrop ND-1000 instrument (Thermo Fisher Scientific Inc., Waltham, MA), and the integrity of these measurements was confirmed using a 2100 BioAnalyzer (Agilent Technologies, South Queensferry, UK). RNA that had an RNA integrity Number (RIN) ≥ 8.6 was used for RNA-Seq.

Library preparation and sequencing

Total RNA was poly(A)-selected using poly(T) Dynabeads (Invitrogen, San Diego, CA). Sequencing libraries were prepared according to Illumina's mRNA-Seq protocol and sequenced at the Omics Science Center (OSC) RIKEN Yokohama Institute. Two independent libraries were analyzed for each data set. Sequence-read data have been submitted to the Sequence Read Archive at DDBJ (submission No. DRA000605).

Mapping and processing of RNA-Seq reads

The reads of each dataset were aligned to the rat reference genome (rn4, Nov. 2004, version 3.4) using TopHat v1.3.0 (Trapnell et al., 2009). The resulting sequence alignment/map files in the BAM format were analyzed with Cufflinks version 0.8.0 (Trapnell et al., 2010) to compute fragments per kilobase of transcript per million mapped reads (FPKM). Genomic annotations were obtained from Ensembl in gene transfer format (GTF). We used only reads mapped to 20 or fewer sites on the genome. The WAD method (Kadota et al., 2008) was then performed on the data of pairs of cells to generate expression differences. Differentially expressed genes were filtered for a WAD ranking cutoff of the

top 5.0%. Gene Ontology (GO) annotations were used to assign biological functions to genes included in this study (Ashburner et al., 2000).

3D Matrigel invasion assay

3D Matrigel invasion assay was performed with a BD BioCoat Matrigel Invasion Chamber (Becton Drive, Franklin Lakes, NJ) according to the manufacturer's protocol. Briefly, 2 x 10^4 cells were seeded on the membrane with or without Matrigel precoating. After 22 hours, cells were fixed, stained for nuclei with propidium iodide, and imaged with an epifluorescence microscope. The number of nuclei was counted with MetaMorph software (Universal Imaging). Data is expressed as the percent invasion through the Matrigel Matrix and membrane relative to the migration through the control membrane.

3D spheroid imaging

Organotypic culture was prepared as described previously (Gaggioli et al., 2007). In a 12-well plate coated with poly-(2-hydroxyethyl methacrylate) (Sigma, St. Louis, MO) and containing 1 ml serum-free CO_2-independent medium (Invitrogen), 10^6 cells were cultured overnight with slow agitation to form small aggregates. The aggregates were embedded in 6 mg/ml Matrigel, maintained in complete medium and observed under a two-photon microscope or a confocal microscope for up to 18 hours in an incubation chamber.

Quantitative RT-PCR

RNA was reverse-transcribed by a High Capacity cDNA Reverse Transcription kit (Applied Biosystems, Foster City, CA) according to the manufacturer's protocol. Then, the expression levels of each gene and GAPDH used as a standard were analyzed by Power SYBR Green PCR Master Mix (Applied Biosystems) with ABI PRISM7300 Sequence Detection System (Applied Biosystems). The sequences of primers used for qPCR are shown in Table S4.

siRNA-Knockdown experiments

Stealth RNAi Negative Control Duplex and Stealth RNAi against MMP15 were purchased from Invitrogen. Mission siRNAs against the other genes were purchased from Sigma-Aldrich (St. Louis, MO). C6 cells stably expressing Raichu-Rac1 were transfected with 20 μM siRNA by Lipofectamine 2000 (Invitrogen). Two days after transfection, cells were used for invasion assay, qPCR, or FRET imaging. The siRNA sequences are shown in Table S5.

Rapamycin-induced Rac1 activation

Rapamycin-induced Rac1 activation with FKBP-Tiam1 was reported previously (Yagi et al., 2012).

Supplementary Materials

Figure S1. (A) Rac1 activity of a single C6 glioma cell and its daughter cells traced for five days. (B) Enrichment of cells in G2/M phases in $Rac1^{low}$ cell populations. (C) Time-lapse analyses of $Rac1^{high}$ and $Rac1^{low}$ cells.

Figure S2. Suppression of Rac1 activity fluctuation by the knockdown of genes enriched in the $Rac1^{high}$ cells.

Figure S3. Effect of Rac1 activation on the expression of invasion-associated genes.

Figure S4. Effect of knockdown of the invasion-associated genes on the expression of the other genes.

Table S1. Genes enriched in $Rac1^{high}$ population and related to "membrane".

Table S2. Transcription factors enriched in $Rac1^{high}$ population.

Table S3. Rac1 activators enriched in $Rac1^{high}$ population.

Table S4. Primer sequences used for qPCR.

Table S5. siRNA sequences.

Movie S1. Slow fluctuation of Rac1 activity during 5-day time-lapse imaging.

Acknowledgments

We thank A. Miyawaki, T. Akagi, J. Miyazaki, K. Yusa, and H. Niwa for the plasmids. Y. Inaoka, K. Hirano, Y. Naruo, K. Takakura and A. Kawagishi are also to be thanked for their technical assistance. We thank F. Hori at Omics Science Center, RIKEN Yokohama Institute and N. Fujii, K Ikeo, and N. Monma at Cell Innovation Project Data Analysis Center, National Institute of Genetics for the sequencing and data analyses. We are grateful to the members of the Matsuda Laboratory for their helpful discussions. MM was supported by the Research Program of Innovative Cell Biology by Innovative Technology (Cell Innovation) from the Ministry of Education, Culture, Sports, and Science (MEXT), Japan. HY was supported by the Global COE Program "Center for Frontier Medicine" and by a Grant-in-Aid for JSPS Fellows by MEXT, Japan.

References

Aoki, K. and Matsuda, M. (2009). Visualization of small GTPase activity with fluorescence resonance energy transfer-based biosensors. Nat. Protoc. 4, 1623-1631.

Ashburner, M., Ball, C. A., Blake, J. A., Botstein, D., Butler, H., Cherry, J. M., Davis, A. P., Dolinski, K., Dwight, S. S., Eppig, J. T. et al. (2000). Gene ontology: tool for the unification of biology. The Gene Ontology Consortium. Nat. Genet. 25, 25-29.

Brock, A., Chang, H. and Huang, S. (2009). Non-genetic heterogeneity--a mutation-independent driving force for the somatic evolution of tumours. Nat.Rev.Genet. 10, 336-342.

Chitu, V., Pixley, F. J., Macaluso, F., Larson, D. R., Condeelis, J., Yeung, Y. G. and Stanley, E. R. (2005). The PCH family member MAYP/PSTPIP2 directly regulates F-actin bundling and enhances filopodia formation and motility in macrophages. Mol.Biol.Cell 16, 2947-2959.

Dai, L., Qin, Z., Defee, M., Toole, B. P., Kirkwood, K. L. and Parsons, C. (2012). Kaposi sarcoma-associated herpesvirus (KSHV) induces a functional tumor-associated phenotype for oral fibroblasts. Cancer Lett. 318, 214-20.

Dason, J. S., Romero-Pozuelo, J., Atwood, H. L. and Ferrus, A. (2012). Multiple roles for Frequenin/NCS-1 in synaptic function and development. Mol.Neurobiol. 45, 388-402.

del Pozo, M. A., Price, L. S., Alderson, N. B., Ren, X. D. and Schwartz, M. A. (2000). Adhesion to the extracellular matrix regulates the coupling of the small GTPase Rac to its effector PAK. EMBO J. 19, 2008-2014.

Dornier, E., Coumailleau, F., Ottavi, J. F., Moretti, J., Boucheix, C., Mauduit, P., Schweisguth, F. and Rubinstein, E. (2012). TspanC8 tetraspanins regulate ADAM10/Kuzbanian trafficking and promote Notch activation in flies and mammals. J. Cell Biol. 199, 481-96.

Etienne-Manneville, S. and Hall, A. (2002). Rho GTPases in cell biology. Nature (London) 420, 629-635.

Gaggioli, C., Hooper, S., Hidalgo-Carcedo, C., Grosse, R., Marshall, J. F., Harrington, K. and Sahai, E. (2007). Fibroblast-led collective invasion of carcinoma cells with differing roles for RhoGTPases in leading and following cells. Nat.Cell Biol. 9, 1392-1400.

Gomez, d. P., Bandres, E., Espina, C., Valdes-Mora, F., Perez-Palacios, R., Garcia-Amigot, F., Garcia-Foncillas, J. and Lacal, J. C. (2007). Differential expression of Rac1 identifies its target genes and its contribution to progression of colorectal cancer. Int.J Biochem.Cell Biol. 39, 2289-2302.

Gotoh, T., Hattori, S., Nakamura, S., Kitayama, H., Noda, M., Takai, Y., Kaibuchi, K., Matsui, H., Hatase, O., Takahashi, H. et al. (1995). Identification of Rap1 as a target for Crk SH3 domain-binding guanine nucleotide-releasing factor, C3G. Mol. Cell Biol. 15, 6746-6753.

Grobben, B., De Deyn, P. P. and Slegers, H. (2002). Rat C6 glioma as experimental model system for the study of glioblastoma growth and invasion. Cell Tissue Res. 310, 257-270.

Haining, E. J., Yang, J., Bailey, R. L., Khan, K., Collier, R., Tsai, S., Watson, S. P., Frampton, J., Garcia, P. and Tomlinson, M. G. (2012). The TspanC8 subgroup of tetraspanins interacts with A disintegrin and metalloprotease 10 (ADAM10) and regulates its maturation and cell surface expression. J. Biol. Chem. 287, 39753-65.

Heasman, S. J. and Ridley, A. J. (2008). Mammalian Rho GTPases: new insights into their functions from in vivo studies. Nat Rev.Mol.Cell Biol. 9, 690-701.

Heppner, G. H. (1984). Tumor heterogeneity. Cancer Res. 44, 2259-2265.

Hirata, E., Yukinaga, H., Kamioka, Y., Arakawa, Y., Miyamoto, S., Okada, T., Sahai, E. and Matsuda, M. (2012). In vivo fluorescence resonance energy transfer imaging reveals differential activation of Rho-family GTPases in glioblastoma cell invasion J. Cell Sci. 125, 858-868.

Itoh, R. E., Kurokawa, K., Ohba, Y., Yoshizaki, H., Mochizuki, N. and Matsuda, M. (2002). Activation of Rac and Cdc42 video-imaged by FRET-based single-molecule probes in the membrane of living cells. Mol. Cell Biol. 22, 6582-6591.

Kadota, K., Nakai, Y. and Shimizu, K. (2008). A weighted average difference method for detecting differentially expressed genes from microarray data. Algorithms.Mol.Biol. 3, 8.

Kamioka, Y., Sumiyama, K., Mizuno, R., Sakai, Y., Hirata, E., Kiyokawa, E. and Matsuda, M. (2012). Live imaging of protein kinase activities in transgenic mice expressing FRET biosensors. Cell Struct. Funct. 37, 65-73.

Kim, D. H., Muto, M., Kuwahara, Y., Nakanishi, Y., Watanabe, H., Aoyagi, K., Ogawa, K., Yoshida, T. and Sasaki, H. (2006). Array-based comparative genomic hybridization of circulating esophageal tumor cells. Oncol. Rep. 16, 1053-9.

Kiyokawa, E., Hara, S., Nakamura, T. and Matsuda, M. (2006). Fluorescence (Forster) resonance energy transfer imaging of oncogene activity in living cells. Cancer Sci. 97, 8-15.

Komatsu, N., Aoki, K., Yamada, M., Yukinaga, H., Fujita, Y., Kamioka, Y. and Matsuda, M. (2011). Development of an optimized backbone of FRET biosensors for kinases and GTPases. Mol. Biol. Cell 22, 4647-4656.

Kraynov, V. S., Chamberlain, C., Bokoch, G. M., Schwartz, M. A., Slabaugh, S. and Hahn, K. M. (2000). Localized rac activation dynamics visualized in living cells. Science 290, 333-337.

Lampert, K., Machein, U., Machein, M. R., Conca, W., Peter, H. H. and Volk, B. (1998). Expression of matrix metalloproteinases and their tissue inhibitors in human brain tumors. Am.J Pathol. 153, 429-437.

Lengauer, C., Kinzler, K. W. and Vogelstein, B. (1998). Genetic instabilities in human cancers. Nature (London) 396, 643-649.

Liu, C. J., Liu, T. Y., Kuo, L. T., Cheng, H. W., Chu, T. H., Chang, K. W. and Lin, S. C. (2008). Differential gene expression signature between primary and metastatic head and neck squamous cell carcinoma. J. Pathol. 214, 489-97.

Louis, D. N. (2006). Molecular pathology of malignant gliomas. Annu.Rev.Pathol. 1, 97-117.

Mack, N. A., Whalley, H. J., Castillo-Lluva, S. and Malliri, A. (2011). The diverse roles of Rac signaling in tumorigenesis. Cell Cycle 10, 1571-1581.

Miyawaki, A. (2011). Development of probes for cellular functions using fluorescent proteins and fluorescence resonance energy transfer. Annu.Rev.Biochem. 80, 357-373.

Mochizuki, S. and Okada, Y. (2007). ADAMs in cancer cell proliferation and progression. Cancer Sci. 98, 621-8.

Nakada, M., Nakamura, H., Ikeda, E., Fujimoto, N., Yamashita, J., Sato, H., Seiki, M. and Okada, Y. (1999). Expression and tissue localization of membrane-type 1, 2, and 3 matrix metalloproteinases in human astrocytic tumors. Am.J Pathol. 154, 417-428.

Nakamura, T. Y., Jeromin, A., Smith, G., Kurushima, H., Koga, H., Nakabeppu, Y., Wakabayashi, S. and Nabekura, J. (2006). Novel role of neuronal Ca2+ sensor-1 as a survival factor up-regulated in injured neurons. J. Cell Biol. 172, 1081-1091.

Parrini, M. C., Sadou-Dubourgnoux, A., Aoki, K., Kunida, K., Biondini, M., Hatzoglou, A., Poullet, P., Formstecher, E., Yeaman, C., Matsuda, M. et al. (2011). SH3BP1, an exocyst-associated RhoGAP, inactivates Rac1 at the front to drive cell motility. Mol. Cell 42, 650-661.

Rubin, H. (1990). The significance of biological heterogeneity. Cancer Metastasis Rev. 9, 1-20.

Sahai, E. and Marshall, C. J. (2002). Rho GTPases and Cancer. Nat.Rev.Cancer 2, 133-142.

Sander, E. E. and Collard, J. G. (1999). Rho-like GTPases: their role in epithelial cell-cell adhesion and invasion. Eur.J.Cancer 35, 1905-1911.

Shackleton, M., Quintana, E., Fearon, E. R. and Morrison, S. J. (2009). Heterogeneity in cancer: cancer stem cells versus clonal evolution. Cell 138, 822-829.

Sigal, A., Milo, R., Cohen, A., Geva-Zatorsky, N., Klein, Y., Liron, Y., Rosenfeld, N., Danon, T., Perzov, N. and Alon, U. (2006). Variability and memory of protein levels in human cells. Nature (London) 444, 643-646.

Singh, D. K., Ku, C. J., Wichaidit, C., Steininger, R. J., III, Wu, L. F. and Altschuler, S. J. (2010). Patterns of basal signaling heterogeneity can distinguish cellular populations with different drug sensitivities. Mol.Syst.Biol. 6, 369.

Tatenhorst, L., Puttmann, S., Senner, V. and Paulus, W. (2005). Genes associated with fast glioma cell migration in vitro and in vivo. Brain Pathol. 15, 46-54.

Teramoto, H., Malek, R. L., Behbahani, B., Castellone, M. D., Lee, N. H. and Gutkind, J. S. (2003). Identification of H-Ras, RhoA, Rac1 and Cdc42 responsive genes. Oncogene 22, 2689-2697.

Trapnell, C., Pachter, L. and Salzberg, S. L. (2009). TopHat: discovering splice junctions with RNA-Seq. Bioinformatics. 25, 1105-1111.

Trapnell, C., Williams, B. A., Pertea, G., Mortazavi, A., Kwan, G., van Baren, M. J., Salzberg, S. L., Wold, B. J. and Pachter, L. (2010). Transcript assembly and quantification by RNA-Seq reveals unannotated transcripts and isoform switching during cell differentiation. Nat Biotechnol. 28, 511-515.

Yagi, S., Matsuda, M. and Kiyokawa, E. (2012). Suppression of Rac1 activity at the apical membrane of MDCK cells is essential for cyst structure maintenance. EMBO Rep. 13, 237-243.

Yoshizaki, H., Ohba, Y., Kurokawa, K., Itoh, R. E., Nakamura, T., Mochizuki, N., Nagashima, K. and Matsuda, M. (2003). Activity of Rho-family GTPases during cell division as visualized with FRET-based probes. J. Cell Biol. 162, 223-232.

Yusa, K., Rad, R., Takeda, J. and Bradley, A. (2009). Generation of transgene-free induced pluripotent mouse stem cells by the piggyBac transposon. Nat.Methods 6, 363-369.

Figure Legends

Fig. 1. Activity variation of Rac1. (A) Schematic view of the Raichu-Rac1 FRET biosensor. (B) C6 glioma cells that stably expressed Raichu-Rac1 were grown on glass-bottom dishes and imaged to visualize the FRET/CFP ratio in the intensity-display mode with the FRET/CFP ratio ranges as indicated in the figures. Bar, 200 μm. (C) The FRET/CFP ratio averaged for each cell in (B) is shown in the histogram, which could be normal distribution (p=0.92, Kolmogorov-Smirnov test and p=0.3, Shapiro-Wilk normality test). Analyses were performed by R(R Ver 2.12.1). (D) The FRET/CFP ratio and YFP intensity in each cell are plotted to show the independence of the Rac1 activity from the concentration of the biosensor.

Fig. 2. Fluctuation and Robustness of Rac1 activity. (A) C6 glioma cells expressing Raichu-Rac1 were plated on glass-bottom dishes with parent C6 glioma cells, which served as feeder cells at a low cell density. Cells were time-lapse imaged for 5 days (Supplementary Movie 1). Representative snap shots of FRET/CFP images and DIC images overlaid with FRET/CFP image are shown. (B) The time course of a single cell and its derivatives after smoothing by the Savitzky-Golay filter, except for the mitosis phase, during which period a surge of Rac1 activity was observed (asterisks and thin lines). The color of each arrow is used to depict each newborn cell. The data are also shown in Supplementary Fig. S1. (C) Power spectrum of Rac1 activity. Blue and red lines indicate normalized power spectra of analyzed cells (N = 58) and the average, respectively. (D) Correlation of Rac1 activities before and after cell division. (E) Scatter plots show the relationship between Rac1 activity and the cell area and velocity of cells. (F) C6 glioma cells expressing Raichu-Rac1 in serum-free media were time-lapse-imaged. During the imaging, 1.25% Trypsin was added at 0.5 h. At 0.75 h, FBS was added to inactivate Trypsin. Bars, 20 μm.

Fig. 3. Isolation of $Rac1^{high}$ and $Rac1^{low}$ cell populations by FACS. (A) C6 glioma cells expressing Raichu-Rac1 were analyzed by FACS. The Rac1 activity (FRET/CFP) did not correlate with the FRET biosensor concentration (YFP) in each cell. (B) The top and bottom 10% of cells were sorted to obtain $Rac1^{high}$ (red) and $Rac1^{low}$ (blue) populations. Small fractions of $Rac1^{high}$ and $Rac1^{low}$ cells were reanalyzed after sorting. (C) $Rac1^{high}$ and $Rac1^{low}$ cells were collected and analyzed by pulldown assay. Cells expressing CFP-Rac1V12 and CFP-Rac1N17 were used as positive and negative controls, respectively. (D) $Rac1^{high}$ and $Rac1^{low}$ cells were plated on dishes and cultured for 3 hours. Cells were labeled with $^{32}P_i$ for 2 hours, lysed, and immunoprecipitated with an anti-GFP antibody, followed by TLC to quantify GTP and GDP bound to the FRET biosensor. . (E) $Rac1^{high}$ and $Rac1^{low}$ cells were used for the Matrigel invasion assay. (F) $Rac1^{high}$, $Rac1^{low}$ cells,

Cdc42^{high}, and Cdc42^{low} cells were plated on dishes and cultured for the indicated periods and re-analyzed by FACS.

Fig. 4. RNA-Seq analysis of Rac1^{high} and Rac1^{low} cell populations. (A) poly(A)-selected RNA was isolated from Rac1^{high} and Rac1^{low} cell populations and used for RNA-Seq analysis. The relationship between average expression [log2(Rac1^{high}×Rac1^{low}) / 2] and expression difference of Rac1^{high} vs Rac1^{low} [log2(Rac1^{high}/Rac1^{low})] is shown in the M-A plot. The WAD method identified 713 differentially expressed genes using cutoffs of the top 5% ranked genes. Cell populations enriched in Rac1^{high} and Rac1^{low} cells are depicted with pink and blue dots, respectively. The top 14 genes for the cellular component term "membrane" are marked in orange, except for Pstpip2, Freq/NCS-1, MMP15, and Tsn17, which are shown with red dots. Elmo1 and Egr2 are shown in green dots. (B) RNA-Seq analysis was similarly performed for the Cdc42^{high}, Cdc42^{low}, RhoA^{high}, and RhoA^{low} cell populations. Scatter plots of the expression differences are shown. (C and D) Gene ontology analysis with biological process terms (C) or cellular component terms (D) is shown. The p-value was calculated by Pearson product-moment correlation coefficients.

Fig. 5. Effect of knockdown of genes enriched in the Rac1^{high} cell population on invasion and Rac1 activity. (A) For the top 14 genes enriched in the cellular component term "membrane", three siRNAs for each gene were prepared and used to knockdown the target genes in C6 glioma cells. Cells were used for invasion analysis as described in the text. The results of two independent experiments are included. *P<0.05, **P<0.01 and ***P<0.001. P-value was calculated by two-tailed paired t-test. (B) Four genes associated with invasion phenotype in (A) and Lgals3 and Rgs2 used as controls were knocked down and FRET/CFP ratio values were quantified for each C6 glioma cells. Numbers of cells analyzed are shown at the bottom. (C) Representative snap shots of FRET/CFP images of C6 glioma cells transfected with the siRNAs. Bars, 100 μm. (D, E, F) Effect of knockdown of Egr2, Elmo1, and PRex1 was also examined as in (A), (B), and (C). Bars, 100 μm.

Fig. 6. Identification of a signaling network comprising the genes enriched in the Rac1^{high} cell population and associated with invasion. (A, B) C6 glioma cells expressing Raichu-Rac1 alone or Raichu-Rac1, plasma membrane-targeted Lyn-FKBP12-rapamycin-binding domain (LDR) and FK506-binding protein (FKBP) fused with Tiam1 were stimulated with (solid line) 10 μM rapamycin or the solvent DMSO (dashed line) for 30 min. Rac1 activity was examined with FACSAria (A) or by pulldown assay (B). C6 glioma cells expressing CFP-Rac1N17 and CFP-Rac1V12 were used as negative and positive controls, respectively. White and black arrows indicate CFP-Rac1 and endogenous Rac1, respectively. Densitometry for GTP-bound Rac1 was normalized to the

amount of the total Rac1.(C) Genes listed in the left column were knocked down as in Fig. 5 or Rac1 was activated as in (A). mRNAs purified from the cells were used for qPCR analysis for the genes in the top row. Fold changes to the control siRNA-transfected cells are shown in the log(2) scale. The genes were clustered by nearest neighbor method. Data on invasion and Rac1 activity shown in Fig. 5 are also included. (D) A proposed model of Rac1 activity regulation in C6 glioma cells.

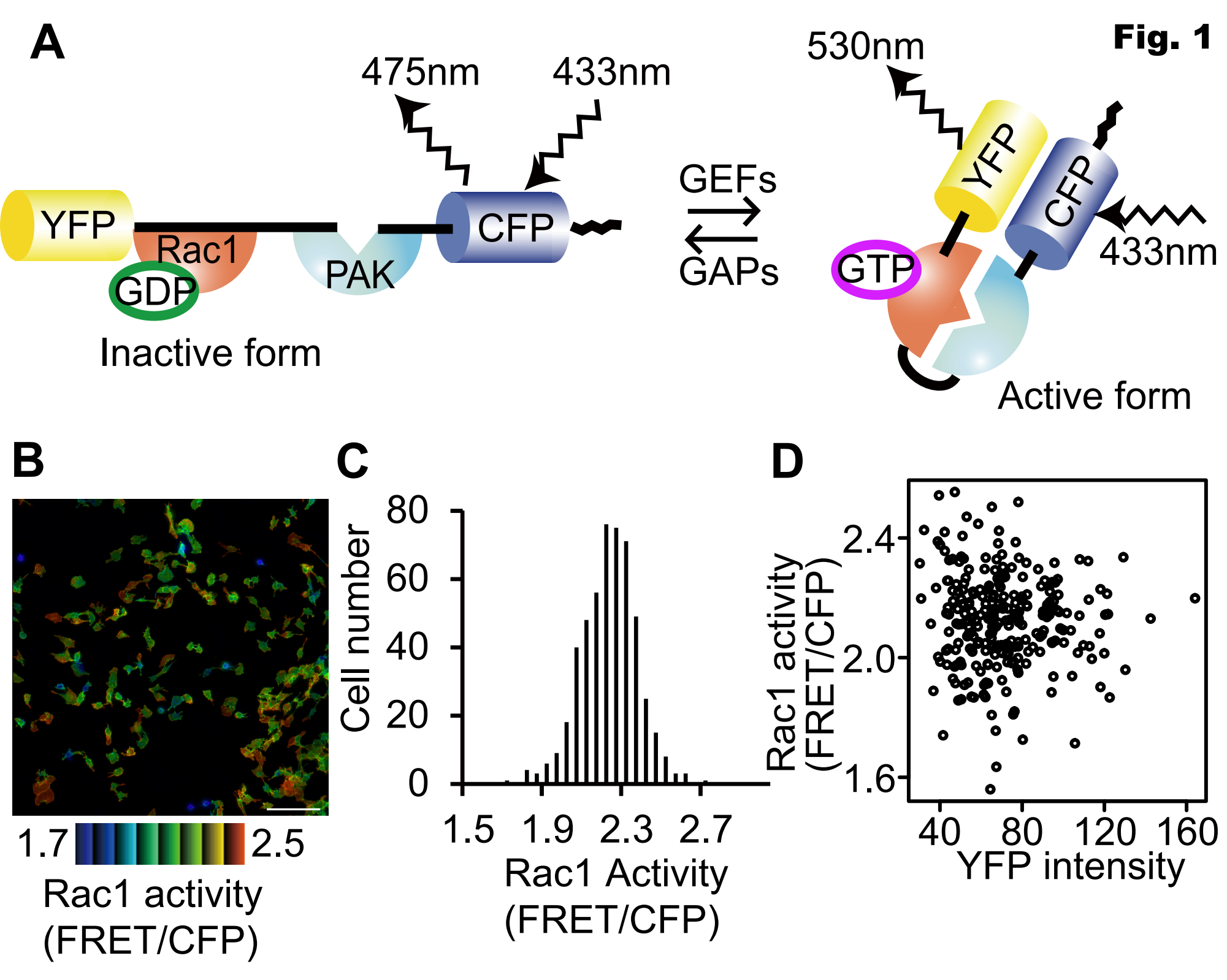
A
Fig. 1
475nm
433nm
YFP
Rac1
GDP
PAK
CFP
Inactive form
GEFs
GAPs
530nm
YFP
CFP
433nm
GTP
Active form
B
1.7
2.5
Rac1 activity
(FRET/CFP)
C
Cell number
80
60
40
20
0
1.5
1.9
2.3
2.7
Rac1 Activity
(FRET/CFP)
D
Rac1 activity
(FRET/CFP)
2.4
2.0
1.6
40
80
120
160
YFP intensity

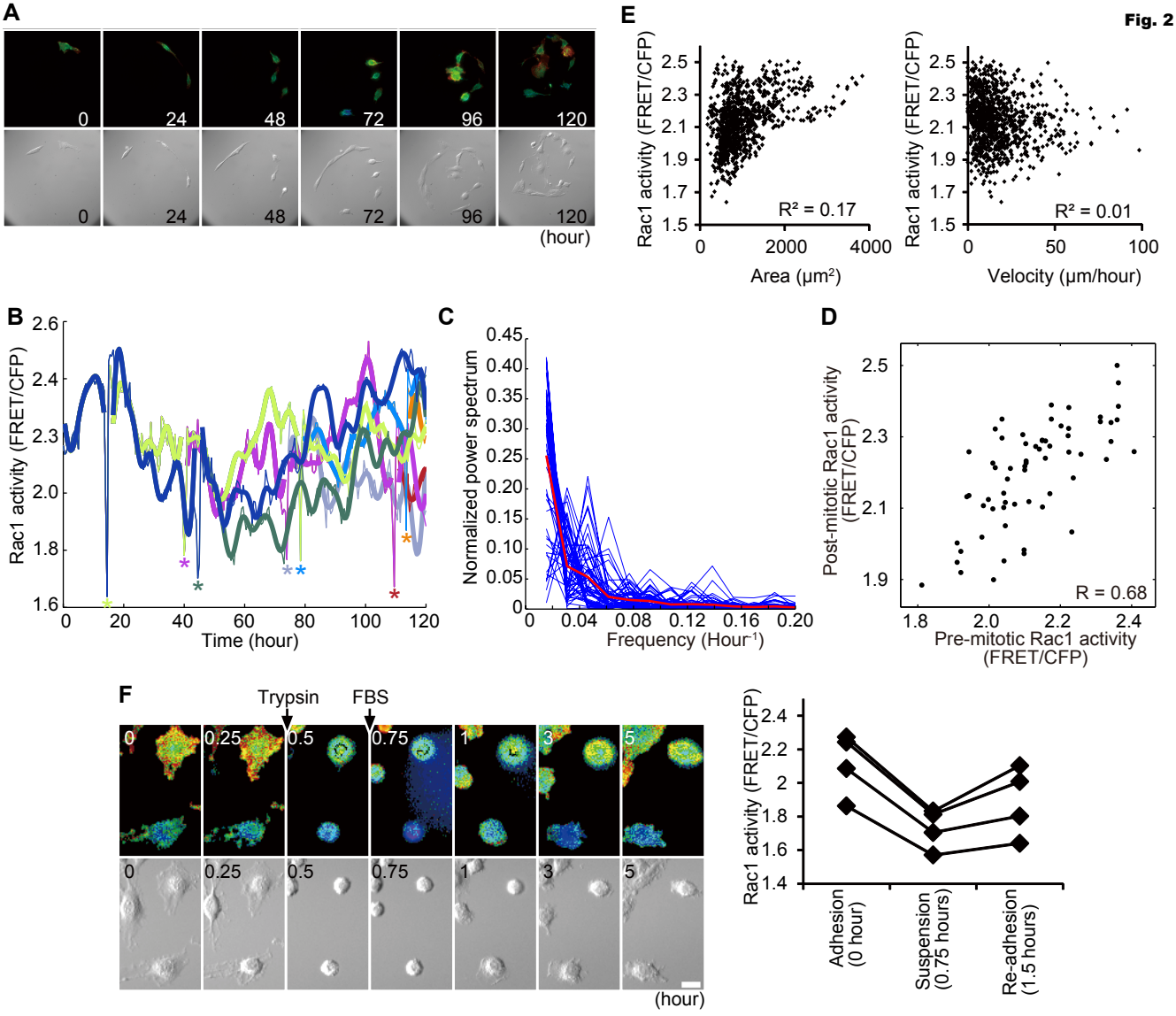
A
0
24
48
72
96
120
(hour)
E
Rac1 activity (FRET/CFP)
R² = 0.17
Area (μm²)
R² = 0.01
Velocity (μm/hour)
B
Rac1 activity (FRET/CFP)
Time (hour)
C
Normalized power spectrum
Frequency (Hour⁻¹)
D
Post-mitotic Rac1 activity (FRET/CFP)
R = 0.68
Pre-mitotic Rac1 activity (FRET/CFP)
F
Trypsin
FBS
0
0.25
0.5
0.75
1
3
5
(hour)
Rac1 activity (FRET/CFP)
Adhesion (0 hour)
Suspension (0.75 hours)
Re-adhesion (1.5 hours)

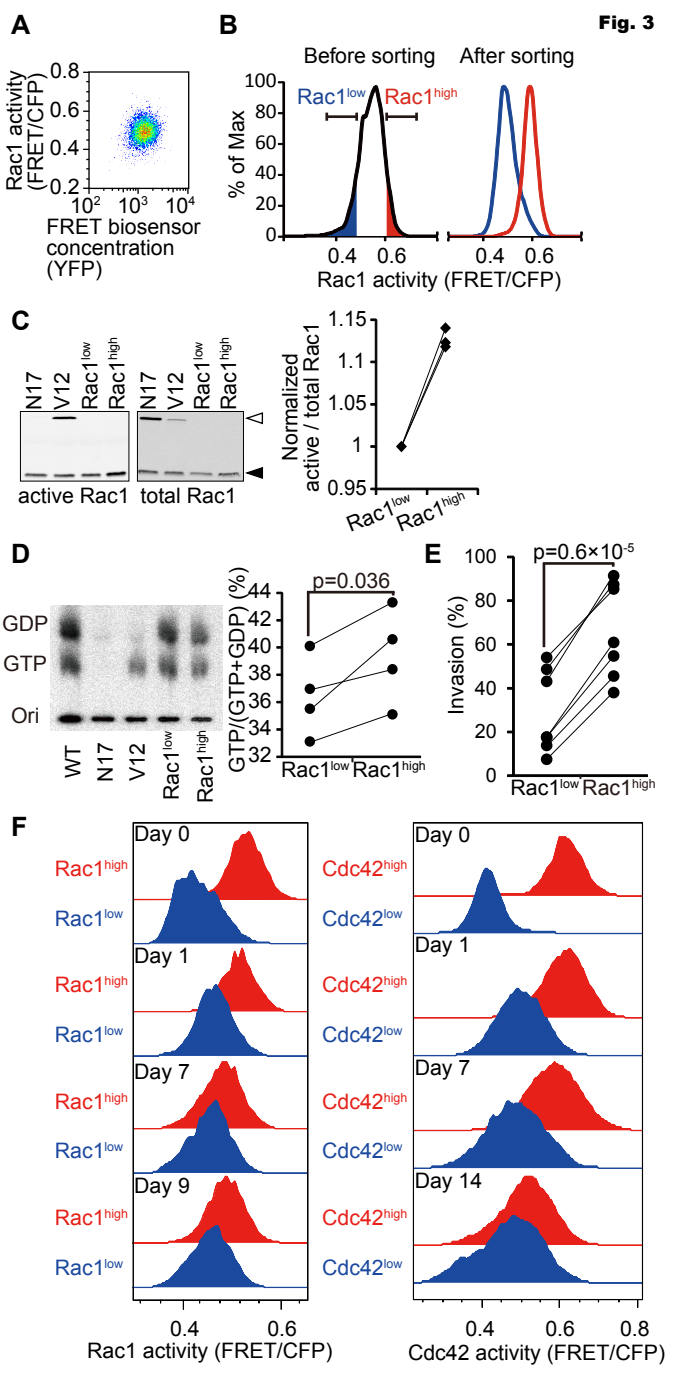
A
Rac1 activity (FRET/CFP)
0.8
0.6
0.4
0.2
10^2
10^3
10^4
FRET biosensor concentration (YFP)
B
Before sorting
After sorting
Rac1low
Rac1high
% of Max
100
80
60
40
20
0
0.4
0.6
Rac1 activity (FRET/CFP)
C
N17
V12
Rac1low
Rac1high
active Rac1
total Rac1
Normalized active / total Rac1
1.15
1.1
1.05
1
0.95
D
GDP
GTP
Ori
WT
N17
V12
Rac1low
Rac1high
GTP/(GTP+GDP) (%)
44
42
40
38
36
34
32
p=0.036
E
Invasion (%)
100
80
60
40
20
0
p=0.6×10-5
F
Day 0
Day 1
Day 7
Day 9
Day 14
Rac1high
Rac1low
Cdc42high
Cdc42low
0.4
0.6
0.8
Rac1 activity (FRET/CFP)
Cdc42 activity (FRET/CFP)

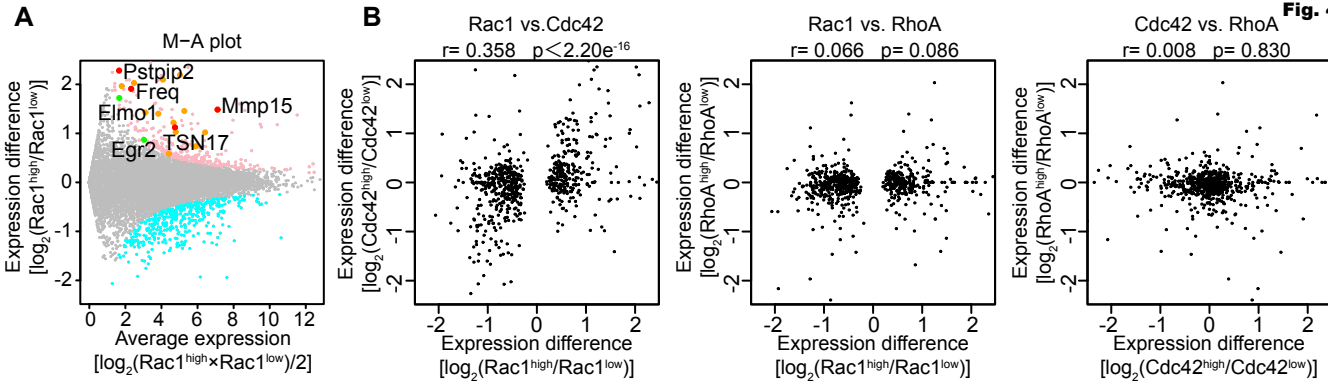

C

Genes up-regulated in $Rac1^{high}$ population

Biological Process	Count	P-value
G-protein coupled receptor protein signaling pathw ay	4	7.36E-07
cell-matrix adhesion	6	3.94E-05
electron transport chain	6	7.55E-05
cellular response to mycophenolic acid	5	1.60E-04
Rac protein signal transduction	3	1.60E-04
positive regulation of endothelial cell proliferation	2	1.64E-04
negative regulation of MAP kinase activity	2	4.09E-04
bioluminescence	4	4.77E-04
glial cell migration	2	9.46E-04
ureteric bud development	4	1.47E-03

Genes up-regulated in $Rac1^{low}$ population

Biological Process	Count	P-value
cell division	24	3.81E-18
cell cycle	30	7.77E-18
mitosis	21	1.19E-16
G-protein coupled receptor protein signaling pathw ay	5	2.43E-10
G1/S transition of mitotic cell cycle	8	2.37E-07
regulation of cell cycle	9	5.35E-06
organ regeneration	9	6.03E-06
positive regulation of cell cycle cytokinesis	4	7.46E-06
mitotic cell cycle	4	9.77E-05
signal transduction	28	1.54E-04

D

Genes up-regulated in $Rac1^{high}$ population

Cellular Component	Count	P-value
respiratory chain	5	2.94E-05
focal adhesion	7	1.21E-04
mitochondrial respiratory chain complex I	4	4.09E-04
cytoplasmic vesicle membrane	5	4.63E-04
Golgi membrane	9	8.99E-04
mitochondrial membrane	5	9.81E-04
membrane	57	1.45E-03
endoplasmic reticulum	18	2.50E-03
Golgi apparatus	17	2.60E-03
integrin complex	3	3.78E-03

Genes up-regulated in $Rac1^{low}$ population

Cellular Component	Count	P-value
cytoplasm	114	1.79E-09
nucleus	110	9.47E-08
integral to membrane	40	1.90E-07
spindle pole	9	1.06E-06
extracellular matrix	15	1.72E-06
centrosome	17	2.63E-06
spindle	9	2.85E-06
chromosome	13	1.90E-05
cytoskeleton	19	1.74E-04
microtubule	11	4.57E-04

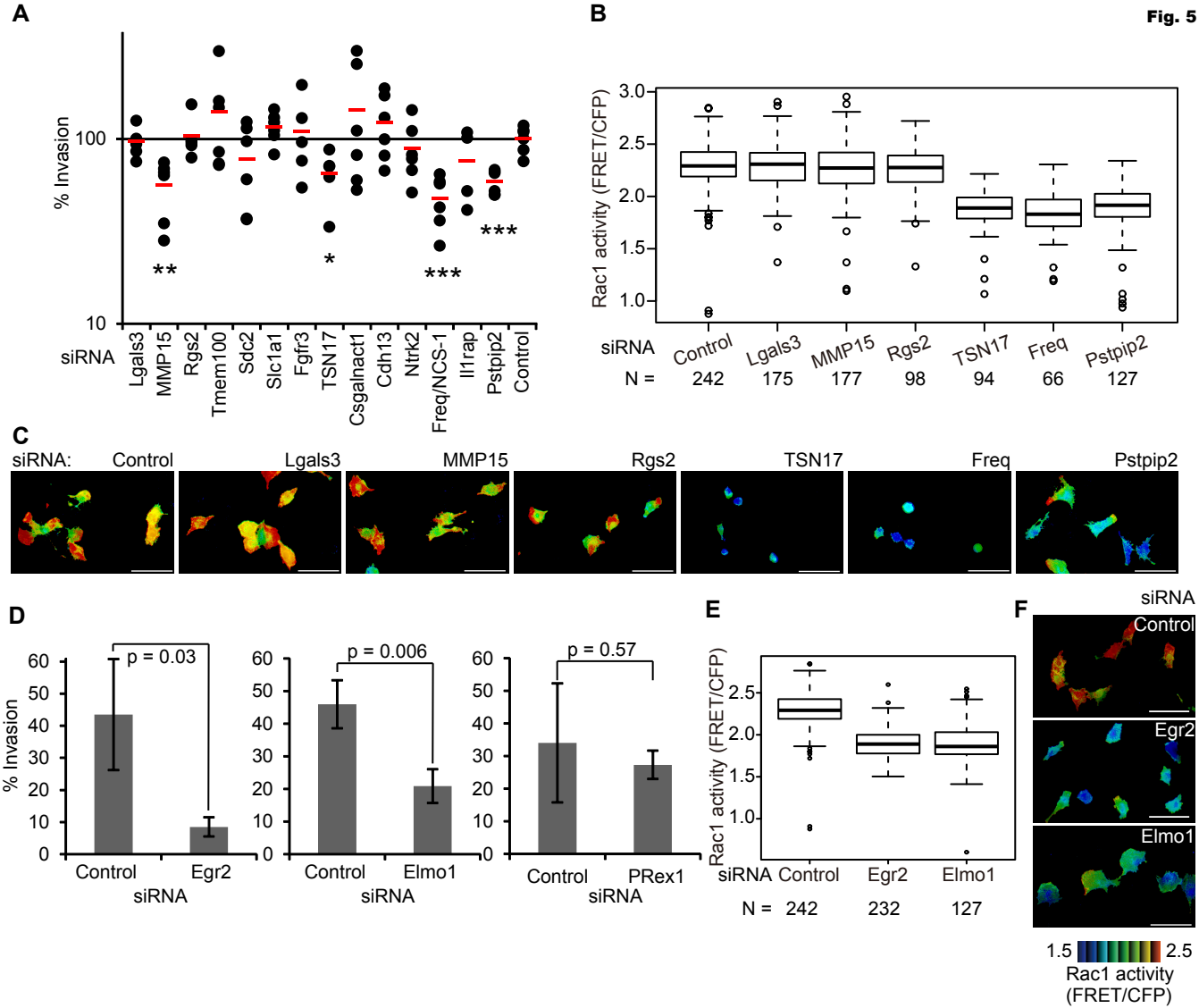
A
% Invasion
100
10
**
*
***
***
siRNA
Lgals3
MMP15
Rgs2
Tmem100
Sdc2
Slc1a1
Fgfr3
TSN17
Csgalnact1
Cdh13
Ntrk2
Freq/NCS-1
Il1rap
Pstpip2
Control
B
Rac1 activity (FRET/CFP)
3.0
2.5
2.0
1.5
1.0
siRNA
Control
Lgals3
MMP15
Rgs2
TSN17
Freq
Pstpip2
N =
242
175
177
98
94
66
127
C
siRNA:
Control
Lgals3
MMP15
Rgs2
TSN17
Freq
Pstpip2
D
% Invasion
p = 0.03
p = 0.006
p = 0.57
Control
Egr2
Elmo1
PRex1
siRNA
E
Rac1 activity (FRET/CFP)
siRNA
Control
Egr2
Elmo1
N =
242
232
127
F
siRNA
Control
Egr2
Elmo1
1.5
2.5
Rac1 activity
(FRET/CFP)

A

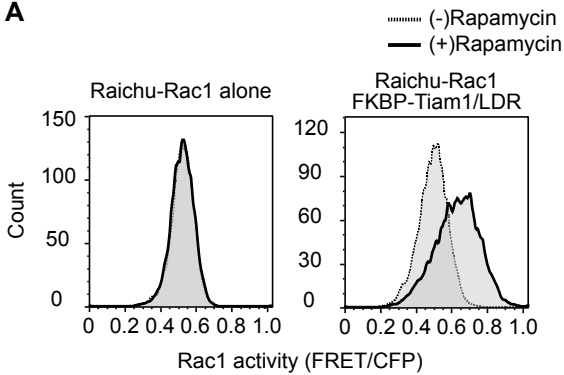

B

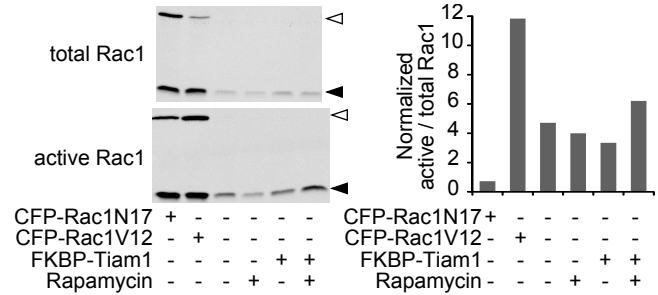

C

		mRNA								Invasion	Rac1 activity
		Rgs2	Lgals3	Egr2	Elmo1	Pstpip2	TSN17	Freq	MMP15		
Activation of Rac1		0.40	-0.34	1.86	0.14	-0.40	0.17	0.25	0.07		0.34
siRNA	Rgs2	-3.60	1.19	0.77	0.15	0.16	-0.94	-0.06	0.99	0.05	-0.01
	Lgals3	-0.33	-3.52	-0.13	0.61	-0.52	0.06	0.04	-0.83	-0.05	0.01
	Egr2	1.06	-0.07	-2.23	0.06	-0.12	-1.55	-1.44	-1.28	-2.32	-0.28
	Elmo1	-1.07	0.63	0.79	-1.99	-1.13	1.20	-0.03	-0.64	-1.25	-0.30
	Pstpip2	-1.61	0.82	0.09	0.62	-3.84	1.68	-0.24	0.87	-0.77	-0.26
	TSN17	1.90	0.65	1.16	0.92	0.30	-5.76	-0.14	-2.48	-0.62	-0.28
	Freq	2.22	1.23	2.91	2.19	1.30	0.97	-4.39	-0.28	-1.07	-0.32
	MMP15	1.06	0.72	3.10	1.97	0.57	0.28	0.14	-4.82	-0.84	-0.01

D

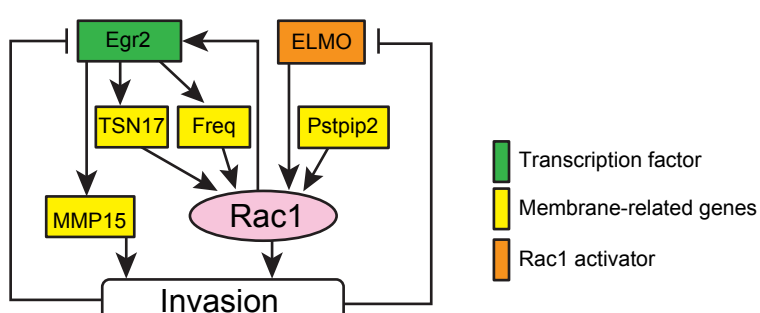

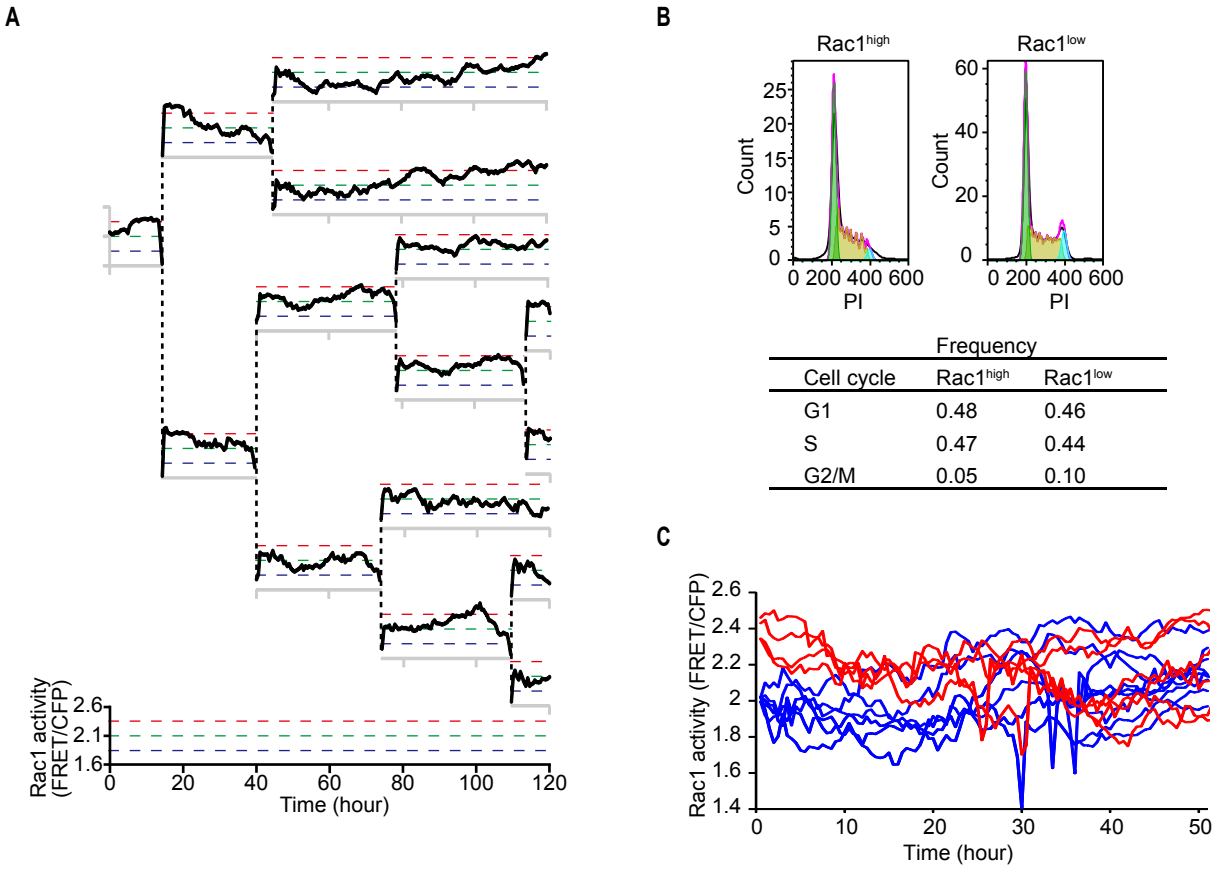

Cell cycle	Rac1^{high}	Rac1^{low}
G1	0.48	0.46
S	0.47	0.44
G2/M	0.05	0.10

Figure S1. (A) Rac1 activity of a single C6 glioma cell and its daughter cells traced for five days. This figure corresponds to Fig. 2B in the text. The red, green, and blue dotted lines indicate FRET/CFP ratios of 2.35, 2.1, and 1.85, respectively. (B) Enrichment of cells in G2/M phases in Rac1^{low} cell populations. Rac1^{high} and Rac1^{low} cells were fixed, stained with propidium iodide (PI), and analyzed by FACS. The pink lines represent fitting by the Watson-Pragmatic cell cycle model. Green, yellow and blue area indicate G1, S, and G2/M phases, respectively. (C) Time-lapse analyses of Rac1^{high} and Rac1^{low} cells.Figure S1. C6 glioma cells expressing Raichu-Rac1 were plated on glass-bottom dishes and time-lapse imaged for 5 days. Cells in the highest (red) and lowest (blue) decile with respect to the FRET/CFP ratio were selected and followed up to 50 hours.

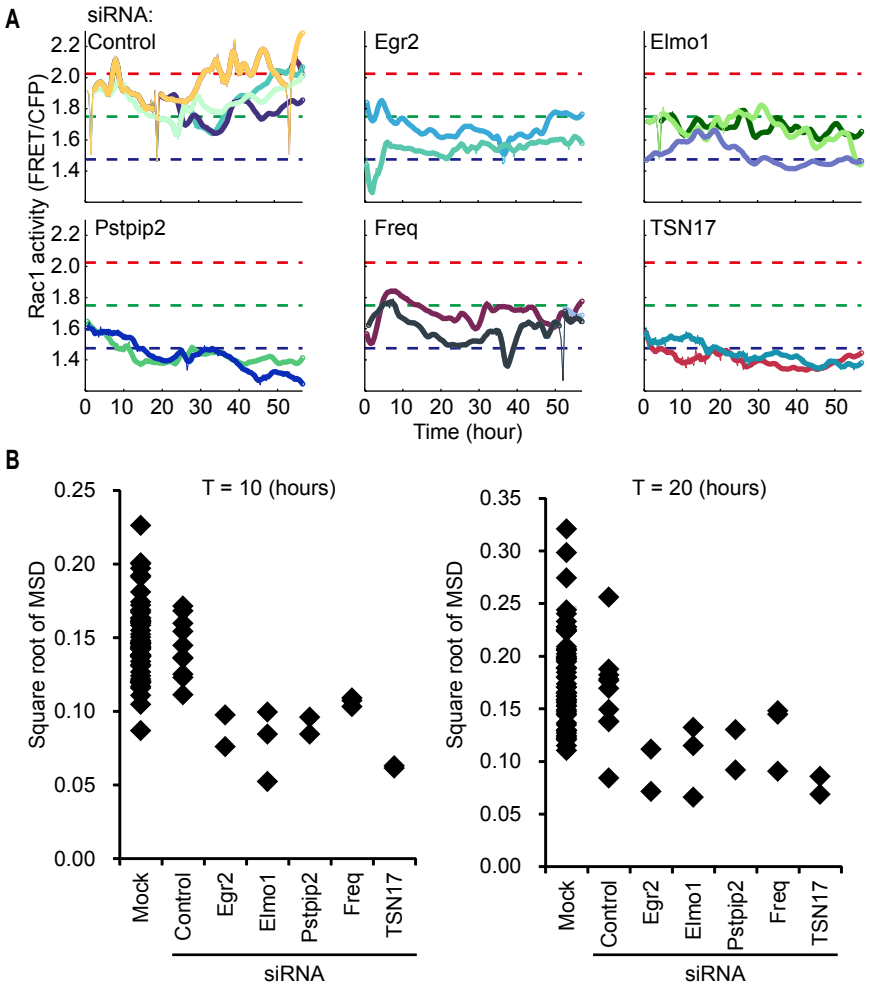

Figure S2. Suppression of Rac1 activity fluctuation by the knockdown of genes enriched in the Rac1^{high} cells. (A) Egr2, Elmo1, Pstpip2, Freq, or TSN17 were knocked down as described in the legend to Fig. 5, followed by time-lapse imaging for at least 50 hours. (B) The time courses are smoothed by the Savitzky-Golay filter, except for the mitosis phase, during which a surge of Rac1 activity was observed. The effect of siRNA-knockdown was evaluated by square root of mean-square displacement (MSD) of the Rac1 activity during 10 or 20 hours window.

$$MSD = \frac{\sum_{t=1}^{T_{end}-T} \{x_{t+T} - x_t\}^2}{T_{end} - T},$$

where xt+T and xt indicate Rac1 activity at time t+T and t, respectively, Tend indicates total duration of imaging, and T is an arbitrary number of duration.

$X = \sqrt{MSD}$,

where X indicates square root of MSD. These analyses were implemented in Matlab software (The Mathworks).

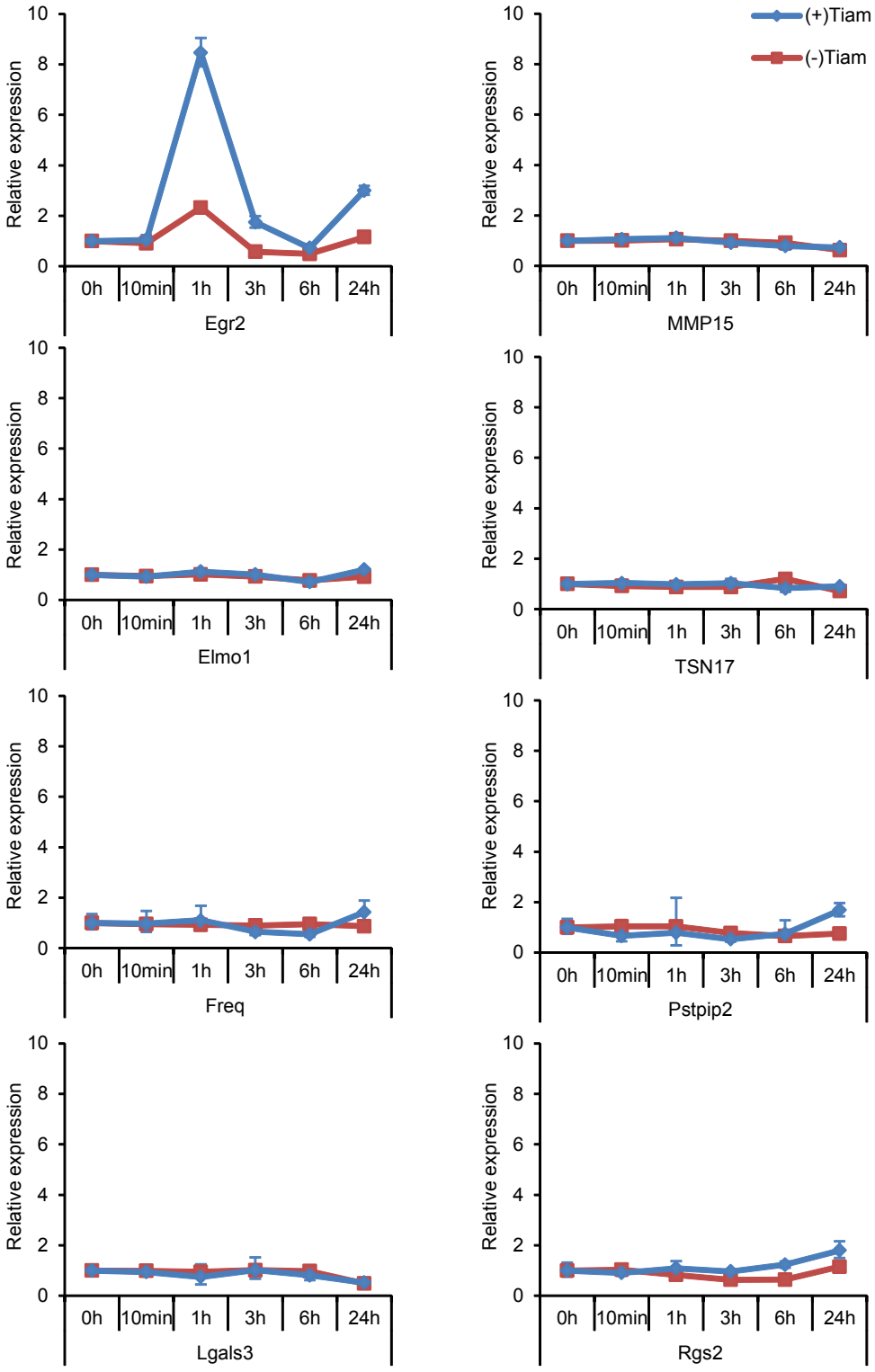

Figure S3. Effect of Rac1 activation on the expression of invasion-associated genes. C6 glioma cells expressing plasma membrane-targeted FKBP12-rapamycin-binding domain, and FK506-binding protein (FKBP) alone or FKBP fused with Tiam1 (blue) or without Tiam1 (red) were stimulated with 10 μM Rapamycin. mRNAs depicted at the bottom were quantified by real-time PCR.

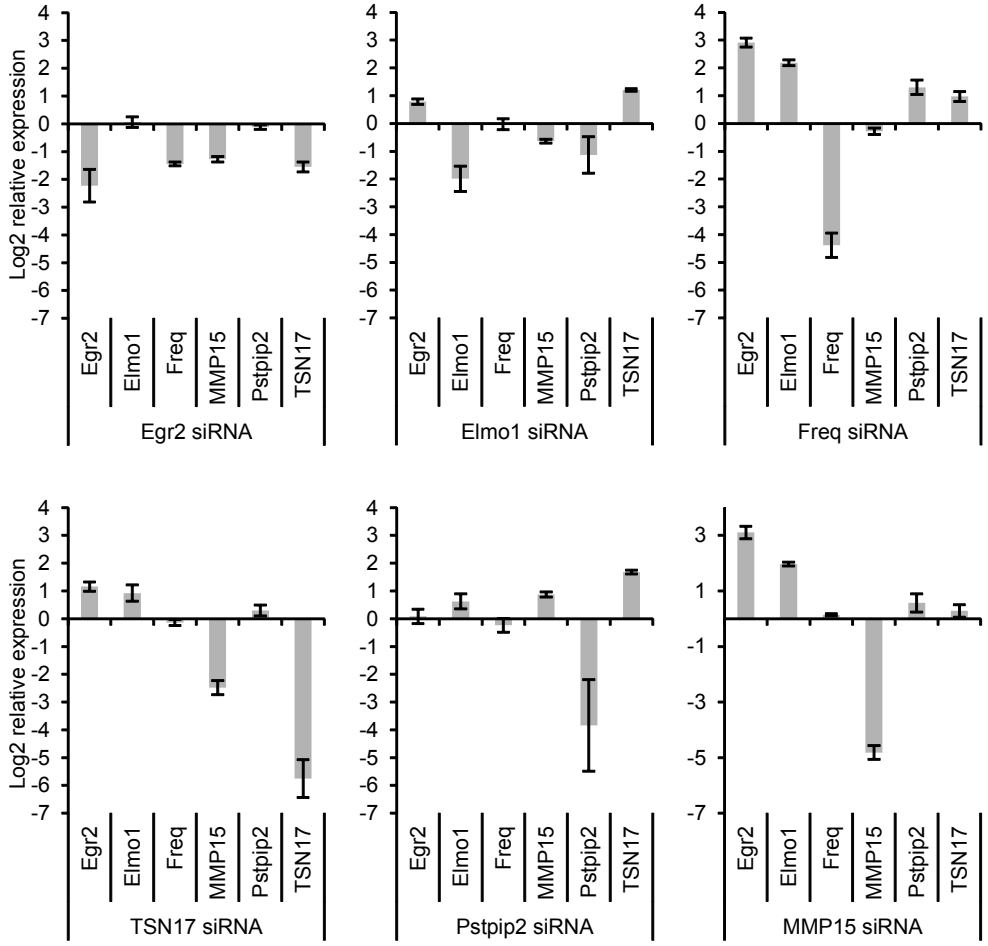

Figure S4. Effect of knockdown of the invasion-associated genes on the expression of the other genes. Genes listed at the bottom were knocked down by siRNAs. mRNAs purified from the cells were analyzed by qPCR for the listed genes. Fold changes to the control siRNA-transfected cells are shown in the log(2) scale. Bars, S.D.

Table S1. Genes enriched in Rac1high population and related to "membrane".

Ensembl gene ID	Symbol	Rac1 experiments					Cdc42	References related to invasion
		Effect of knockdown on invasion*	WAD rank	RNA-Seq** Exp.1	RNA-Seq** Exp.2	qPCR	RNA-Seq	
ENSRNOG00000010645	Lgals3	→	10	3.06	6.83	2.07	0.96	1-9
ENSRNOG00000012622	Mmp15	↓	12	2.01	3.89	3.41	6.78	10-30
ENSRNOG00000003687	Rgs2	→	17	3.14	5.83	2.96	3.00	31-33
ENSRNOG00000018566	Ctsl1	N.A.	21	1.70	2.40	1.63	1.40	34-36
ENSRNOG00000002434	Tmem100	→	26	2.03	3.72	2.61	3.11	
ENSRNOG00000004936	Sdc2	→	38	1.82	2.26	2.02	0.97	37-42
ENSRNOG00000014816	Slc1a1	→	65	2.00	2.71	2.56	5.01	
ENSRNOG00000016818	Fgfr3	→	76	2.08	3.34	2.94	1.83	43-48
ENSRNOG00000018122	TSN17	↓	78	1.75	2.71	2.55	1.21	
ENSRNOG00000013024	Csgalnact1	→	87	2.82	5.91	5.92	1.65	
ENSRNOG00000014371	Cdh13	→	93	1.57	2.64	1.55	1.53	49-57
ENSRNOG00000006756	Maged1	N.A.	105	1.54	1.82	1.31	0.97	58-62
ENSRNOG00000018646	Hbegf	N.A.	112	1.60	1.84	1.42	1.55	63, 64
ENSRNOG00000018839	Ntrk2	→	128	2.86	2.52	2.35	2.08	65-70
ENSRNOG00000008761	Freq	↓	129	3.21	4.40	4.48	0.83	
ENSRNOG00000001928	Il1rap	→	137	1.58	1.76	1.80	2.06	
ENSRNOG00000006646	Ecop	N.A.	144	3.79	4.78	N.D.	1.05	
ENSRNOG00000004322	Sh3kbp1	N.A.	150	1.50	1.90	1.42	1.82	71-74
ENSRNOG00000019536	Nid67	N.A.	152	1.79	1.74	1.74	1.46	
ENSRNOG00000007060	Adfp	N.A.	179	1.31	1.80	1.72	0.98	
ENSRNOG00000009922	Prlhr	N.A.	192	1.30	3.56	4.36	4.16	
ENSRNOG00000007638	Loxl3	N.A.	197	1.18	1.57	1.68	1.44	75, 76
ENSRNOG00000016987	Pstpip2	↓	211	3.80	6.23	5.51	3.07	77

*Effect of knock-down on glioma invasion: See legend to Figure 5 in the main text; ↓, suppressed; →, not affected; N.A., not analyzed

**RNA-Seq was performed twice. Fold increase of $Rac1^{high}$ vs $Rac1^{low}$, or $Cdc42^{high}$ vs $Cdc42^{low}$ cell populations is shown.

References

1 Zeiger MA, Dackiw AP (2005) Follicular thyroid lesions, elements that affect both diagnosis and prognosis. Journal of surgical oncology 89: 108-113

2 Takenaka Y, Fukumori T, Raz A (2004) Galectin-3 and metastasis. Glycoconjugate journal 19: 543-549

3 Seemayer CA, Distler O, Kuchen S, Muller-Ladner U, Michel BA, Neidhart M, Gay RE, Gay S (2001) [Rheumatoid arthritis: new developments in the pathogenesis with special reference to synovial fibroblasts]. Zeitschrift fur Rheumatologie 60: 309-318

4 Newlaczyl AU, Yu LG (2011) Galectin-3--a jack-of-all-trades in cancer. Cancer letters 313: 123-128

5 Larsen L, Chen HY, Saegusa J, Liu FT (2011) Galectin-3 and the skin. Journal of dermatological science 64: 85-91

6 Hornebeck W, Robinet A, Duca L, Antonicelli F, Wallach J, Bellon G (2005) The elastin connection and melanoma progression. Anticancer research 25: 2617-2625

7 Duner S, Lopatko Lindman J, Ansari D, Gundewar C, Andersson R (2010) Pancreatic cancer: the role of pancreatic stellate cells in tumor progression. Pancreatology 10: 673-681

8 Dhirapong A, Lleo A, Leung P, Gershwin ME, Liu FT (2009) The immunological potential of galectin-1 and -3. Autoimmunity reviews 8: 360-363

9 Chen HY, Liu FT, Yang RY (2005) Roles of galectin-3 in immune responses. Archivum immunologiae et therapiae experimentalis 53: 497-504

10 Quick RE, Dunlap JA, Jessen JR (2012) Expression analysis of zebrafish membrane type-2 matrix metalloproteinases during embryonic development. Gene expression patterns : GEP

11 Johnson JL, Pillai S, Pernazza D, Sebti SM, Lawrence NJ, Chellappan SP (2012) Regulation of matrix metalloproteinase genes by E2F transcription factors: Rb-Raf-1 interaction as a novel target for metastatic disease. Cancer research 72: 516-526

12 Tao G, Levay AK, Gridley T, Lincoln J (2011) Mmp15 is a direct target of Snai1 during endothelial to mesenchymal transformation and endocardial cushion development. Developmental biology 359: 209-221

13 Chen L, Di D, Luo G, Zheng L, Tan Y, Zhang X, Xu N (2010) Immunochemical staining of MT2-MMP correlates positively to angiogenesis of human esophageal cancer. Anticancer research 30: 4363-4368

14 Ortega P, Moran A, Fernandez-Marcelo T, De Juan C, Frias C, Lopez-Asenjo JA, Sanchez-Pernaute A, Torres A, Diaz-Rubio E, Iniesta P, Benito M (2010) MMP-7 and SGCE as distinctive molecular factors in sporadic colorectal cancers from the mutator phenotype pathway. International journal of oncology 36: 1209-1215

15 Wang Q, Li M, Wang Y, Zhang Y, Jin S, Xie G, Liu Z, Wang S, Zhang H, Shen L, Ge H (2008) RNA interference targeting CML66, a novel tumor antigen, inhibits proliferation, invasion and metastasis of HeLa cells. Cancer letters 269: 127-138

16 Hiden U, Wadsack C, Prutsch N, Gauster M, Weiss U, Frank HG, Schmitz U, Fast-Hirsch C, Hengstschlager M, Potgens A, Ruben A, Knofler M, Haslinger P, Huppertz B, Bilban M, Kaufmann P, Desoye G (2007) The first trimester human trophoblast cell line ACH-3P: a novel tool to study autocrine/paracrine regulatory loops of human trophoblast subpopulations--TNF-alpha stimulates MMP15 expression. BMC developmental biology 7: 137

17 Bassi DE, Lopez De Cicco R, Cenna J, Litwin S, Cukierman E, Klein-Szanto AJ (2005) PACE4 expression in mouse basal keratinocytes results in basement membrane disruption and acceleration of tumor progression. Cancer research 65: 7310-7319

18 Zhang J, Sarkar S, Yong VW (2005) The chemokine stromal cell derived factor-1 (CXCL12) promotes glioma invasiveness through MT2-matrix metalloproteinase. Carcinogenesis 26: 2069-2077

19 Lafleur MA, Drew AF, de Sousa EL, Blick T, Bills M, Walker EC, Williams ED, Waltham M, Thompson EW (2005) Upregulation of matrix metalloproteinases (MMPs) in breast cancer xenografts: a major induction of stromal MMP-13. International journal of cancer Journal international du cancer 114: 544-554

20 Van Meter TE, Broaddus WC, Rooprai HK, Pilkington GJ, Fillmore HL (2004) Induction of membrane-type-1 matrix metalloproteinase by epidermal growth factor-mediated signaling in gliomas. Neuro-oncology 6: 188-199

21 Rozanov DV, Hahn-Dantona E, Strickland DK, Strongin AY (2004) The low density lipoprotein receptor-related protein LRP is regulated by membrane type-1 matrix metalloproteinase (MT1-MMP) proteolysis in malignant cells. The Journal of biological chemistry 279: 4260-4268

22 Mahloogi H, Bassi DE, Klein-Szanto AJ (2002) Malignant conversion of non-tumorigenic murine skin keratinocytes overexpressing PACE4. Carcinogenesis 23: 565-572

23 Iwasaki M, Nishikawa A, Fujimoto T, Akutagawa N, Manase K, Endo T, Yoshida K, Maekawa R, Yoshioka T, Kudo R (2002) Anti-invasive effect of MMI-166, a new selective matrix metalloproteinase inhibitor, in cervical carcinoma cell lines. Gynecologic oncology 85: 103-107

24 Hotary KB, Yana I, Sabeh F, Li XY, Holmbeck K, Birkedal-Hansen H, Allen ED, Hiraoka N, Weiss SJ (2002) Matrix metalloproteinases (MMPs) regulate fibrin-invasive activity via MT1-MMP-dependent and -independent processes. The Journal of experimental medicine 195: 295-308

25 Ohashi K, Nemoto T, Nakamura K, Nemori R (2000) Increased expression of matrix metalloproteinase 7 and 9 and membrane type 1-matrix metalloproteinase in esophageal squamous cell carcinomas. Cancer 88: 2201-2209

26 Bjorn SF, Hastrup N, Larsen JF, Lund LR, Pyke C (2000) Messenger RNA for membrane-type 2 matrix metalloproteinase, MT2-MMP, is expressed in human placenta of first trimester. Placenta 21: 170-176

27 Ellenrieder V, Alber B, Lacher U, Hendler SF, Menke A, Boeck W, Wagner M, Wilda M, Friess H, Buchler M, Adler G, Gress

TM (2000) Role of MT-MMPs and MMP-2 in pancreatic cancer progression. International journal of cancer Journal international du cancer 85: 14-20

28 Nakamura H, Ueno H, Yamashita K, Shimada T, Yamamoto E, Noguchi M, Fujimoto N, Sato H, Seiki M, Okada Y (1999) Enhanced production and activation of progelatinase A mediated by membrane-type 1 matrix metalloproteinase in human papillary thyroid carcinomas. Cancer research 59: 467-473

29 Theret N, Musso O, L'Helgoualc'h A, Campion JP, Clement B (1998) Differential expression and origin of membrane-type 1 and 2 matrix metalloproteinases (MT-MMPs) in association with MMP2 activation in injured human livers. The American journal of pathology 153: 945-954

30 Gilles C, Polette M, Seiki M, Birembaut P, Thompson EW (1997) Implication of collagen type I-induced membrane-type 1-matrix metalloproteinase expression and matrix metalloproteinase-2 activation in the metastatic progression of breast carcinoma. Laboratory investigation; a journal of technical methods and pathology 76: 651-660

31 Kim HJ, Roh MS, Son CH, Kim AJ, Jee HJ, Song N, Kim M, Seo SY, Yoo YH, Yun J (2012) Loss of Med1/TRAP220 promotes the invasion and metastasis of human non-small-cell lung cancer cells by modulating the expression of metastasis-related genes. Cancer letters 321: 195-202

32 Auburn S, Fry AE, Clark TG, Campino S, Diakite M, Green A, Richardson A, Jallow M, Sisay-Joof F, Pinder M, Molyneux ME, Taylor TE, Haldar K, Rockett KA, Kwiatkowski DP (2010) Further evidence supporting a role for gs signal transduction in severe malaria pathogenesis. PloS one 5: e10017

33 Jiang Z, Wang Z, Xu Y, Wang B, Huang W, Cai S (2010) Analysis of RGS2 expression and prognostic significance in stage II and III colorectal cancer. Bioscience reports 30: 383-390

34 Lankelma JM, Voorend DM, Barwari T, Koetsveld J, Van der Spek AH, De Porto AP, Van Rooijen G, Van Noorden CJ (2010) Cathepsin L, target in cancer treatment? Life sciences 86: 225-233

35 Duffy MJ (1996) Proteases as prognostic markers in cancer. Clinical cancer research : an official journal of the American Association for Cancer Research 2: 613-618

36 Herszenyi L, Plebani M, Carraro P, De Paoli M, Roveroni G, Rugge M, Cardin R, Naccarato R, Farinati F (1995) [Role and behavior of cathepsin B and cathepsin L in gastric cancer]. Orvosi hetilap 136: 1315-1318

37 Baniwal SK, Khalid O, Gabet Y, Shah RR, Purcell DJ, Mav D, Kohn-Gabet AE, Shi Y, Coetzee GA, Frenkel B (2010) Runx2 transcriptome of prostate cancer cells: insights into invasiveness and bone metastasis. Molecular cancer 9: 258

38 Choi Y, Kim H, Chung H, Hwang JS, Shin JA, Han IO, Oh ES (2010) Syndecan-2 regulates cell migration in colon cancer cells through Tiam1-mediated Rac activation. Biochemical and biophysical research communications 391: 921-925

39 Choi S, Kim Y, Park H, Han IO, Chung E, Lee SY, Kim YB, Lee JW, Oh ES, Yi JY (2009) Syndecan-2 overexpression regulates adhesion and migration through cooperation with integrin alpha2. Biochemical and biophysical research communications 384: 231-235

40 Park H, Han I, Kwon HJ, Oh ES (2005) Focal adhesion kinase regulates syndecan-2-mediated tumorigenic activity of HT1080 fibrosarcoma cells. Cancer research 65: 9899-9905

41 Watanabe A, Mabuchi T, Satoh E, Furuya K, Zhang L, Maeda S, Naganuma H (2006) Expression of syndecans, a heparan sulfate proteoglycan, in malignant gliomas: participation of nuclear factor-kappaB in upregulation of syndecan-1 expression. Journal of neuro-oncology 77: 25-32

42 Davies EJ, Blackhall FH, Shanks JH, David G, McGown AT, Swindell R, Slade RJ, Martin-Hirsch P, Gallagher JT, Jayson GC (2004) Distribution and clinical significance of heparan sulfate proteoglycans in ovarian cancer. Clinical cancer research : an official journal of the American Association for Cancer Research 10: 5178-5186

43 Al-Ahmadie HA, Iyer G, Janakiraman M, Lin O, Heguy A, Tickoo SK, Fine SW, Gopalan A, Chen YB, Balar A, Riches J, Bochner B, Dalbagni G, Bajorin DF, Reuter VE, Milowsky MI, Solit DB (2011) Somatic mutation of fibroblast growth factor

receptor-3 (FGFR3) defines a distinct morphological subtype of high-grade urothelial carcinoma. The Journal of pathology 224: 270-279

44 Knuchel-Clarke R, Dahl E, Gaisa NT, Schwamborn K, Lindemann-Docter K, Henkel C (2010) [Current knowledge in molecular pathology of urothelial cancer]. Der Pathologe 31 Suppl 2: 234-238

45 McConkey DJ, Choi W, Marquis L, Martin F, Williams MB, Shah J, Svatek R, Das A, Adam L, Kamat A, Siefker-Radtke A, Dinney C (2009) Role of epithelial-to-mesenchymal transition (EMT) in drug sensitivity and metastasis in bladder cancer. Cancer metastasis reviews 28: 335-344

46 Hofstadter F (2008) [Urothelial carcinoma. Does surgical pathology learn from molecular pathology?]. Der Pathologe 29 Suppl 2: 145-148

47 Wolff EM, Liang G, Jones PA (2005) Mechanisms of Disease: genetic and epigenetic alterations that drive bladder cancer. Nature clinical practice Urology 2: 502-510

48 Iida S, Ueda R (2003) Multistep tumorigenesis of multiple myeloma: its molecular delineation. International journal of hematology 77: 207-212

49 Chung JH, Lee HJ, Kim BH, Cho NY, Kang GH (2011) DNA methylation profile during multistage progression of pulmonary adenocarcinomas. Virchows Archiv : an international journal of pathology 459: 201-211

50 Feng W, Orlandi R, Zhao N, Carcangiu ML, Tagliabue E, Xu J, Bast RC, Jr., Yu Y (2010) Tumor suppressor genes are frequently methylated in lymph node metastases of breast cancers. BMC cancer 10: 378

51 Celebiler Cavusoglu A, Kilic Y, Saydam S, Canda T, Baskan Z, Sevinc AI, Sakizli M (2009) Predicting invasive phenotype with CDH1, CDH13, CD44, and TIMP3 gene expression in primary breast cancer. Cancer science 100: 2341-2345

52 Kuphal S, Martyn AC, Pedley J, Crowther LM, Bonazzi VF, Parsons PG, Bosserhoff AK, Hayward NK, Boyle GM (2009) H-cadherin expression reduces invasion of malignant melanoma. Pigment cell & melanoma research 22: 296-306

53 Kim DS, Kim MJ, Lee JY, Kim YZ, Kim EJ, Park JY (2007) Aberrant methylation of E-cadherin and H-cadherin genes in nonsmall cell lung cancer and its relation to clinicopathologic features. Cancer 110: 2785-2792

54 Qian ZR, Sano T, Yoshimoto K, Asa SL, Yamada S, Mizusawa N, Kudo E (2007) Tumor-specific downregulation and methylation of the CDH13 (H-cadherin) and CDH1 (E-cadherin) genes correlate with aggressiveness of human pituitary adenomas. Modern pathology : an official journal of the United States and Canadian Academy of Pathology, Inc 20: 1269-1277

55 Fukuoka T, Hibi K, Nakao A (2006) Aberrant methylation is frequently observed in advanced esophageal squamous cell carcinoma. Anticancer research 26: 3333-3335

56 Maruyama R, Toyooka S, Toyooka KO, Harada K, Virmani AK, Zochbauer-Muller S, Farinas AJ, Vakar-Lopez F, Minna JD, Sagalowsky A, Czerniak B, Gazdar AF (2001) Aberrant promoter methylation profile of bladder cancer and its relationship to clinicopathological features. Cancer research 61: 8659-8663

57 Kremmidiotis G, Baker E, Crawford J, Eyre HJ, Nahmias J, Callen DF (1998) Localization of human cadherin genes to chromosome regions exhibiting cancer-related loss of heterozygosity. Genomics 49: 467-471

58 Fussbroich B, Wagener N, Macher-Goeppinger S, Benner A, Falth M, Sultmann H, Holzer A, Hoppe-Seyler K, Hoppe-Seyler F (2011) EZH2 depletion blocks the proliferation of colon cancer cells. PloS one 6: e21651

59 Germano S, Kennedy S, Rani S, Gleeson G, Clynes M, Doolan P, McDonnell S, Hughes L, Crown J, O'Driscoll L (2012) MAGE-D4B is a novel marker of poor prognosis and potential therapeutic target involved in breast cancer tumorigenesis. International journal of cancer Journal international du cancer 130: 1991-2002

60 Du Q, Zhang Y, Tian XX, Li Y, Fang WG (2009) MAGE-D1 inhibits proliferation, migration and invasion of human breast cancer cells. Oncology reports 22: 659-665

61 Shen WG, Xue QY, Zhu J, Hu BS, Zhang Y, Wu YD, Su Q (2007b) Inhibition of adenovirus-mediated human MAGE-D1 on

angiogenesis in vitro and in vivo. Molecular and cellular biochemistry 300: 89-99

62 Shen WG, Xue QY, Wu YD, Hu BS, Zhu J, Zhang Y, Su Q (2007a) Melanoma-associated antigen family protein-D1 regulation of tumor cell migration, adhesion to endothelium, and actin structures reorganization in response to hypoxic stress. Cell communication & adhesion 14: 21-31

63 Belo A, Cheng K, Chahdi A, Shant J, Xie G, Khurana S, Raufman JP (2011) Muscarinic receptor agonists stimulate human colon cancer cell migration and invasion. American journal of physiology Gastrointestinal and liver physiology 300: G749-760

64 Wright JK, Dunk CE, Amsalem H, Maxwell C, Keating S, Lye SJ (2010) HER1 signaling mediates extravillous trophoblast differentiation in humans. Biology of reproduction 83: 1036-1045

65 Matsumoto K, Wada RK, Yamashiro JM, Kaplan DR, Thiele CJ (1995) Expression of brain-derived neurotrophic factor and p145TrkB affects survival, differentiation, and invasiveness of human neuroblastoma cells. Cancer research 55: 1798-1806

66 Sclabas GM, Fujioka S, Schmidt C, Li Z, Frederick WA, Yang W, Yokoi K, Evans DB, Abbruzzese JL, Hess KR, Zhang W, Fidler IJ, Chiao PJ (2005) Overexpression of tropomysin-related kinase B in metastatic human pancreatic cancer cells. Clinical cancer research : an official journal of the American Association for Cancer Research 11: 440-449

67 Miyamoto Y, Yamauchi J, Tanoue A, Wu C, Mobley WC (2006) TrkB binds and tyrosine-phosphorylates Tiam1, leading to activation of Rac1 and induction of changes in cellular morphology. Proceedings of the National Academy of Sciences of the United States of America 103: 10444-10449

68 Kupferman ME, Jiffar T, El-Naggar A, Yilmaz T, Zhou G, Xie T, Feng L, Wang J, Holsinger FC, Yu D, Myers JN (2010) TrkB induces EMT and has a key role in invasion of head and neck squamous cell carcinoma. Oncogene 29: 2047-2059

69 Zhang S, Guo D, Luo W, Zhang Q, Zhang Y, Li C, Lu Y, Cui Z, Qiu X (2010) TrkB is highly expressed in NSCLC and mediates BDNF-induced the activation of Pyk2 signaling and the invasion of A549 cells. BMC cancer 10: 43

70 Guo D, Sun W, Zhu L, Zhang H, Hou X, Liang J, Jiang X, Liu C (2012) Knockdown of BDNF suppressed invasion of HepG2 and HCCLM3 cells, a mechanism associated with inactivation of RhoA or Rac1 and actin skeleton disorganization. APMIS : acta pathologica, microbiologica, et immunologica Scandinavica 120: 469-476

71 Nam JM, Onodera Y, Mazaki Y, Miyoshi H, Hashimoto S, Sabe H (2007) CIN85, a Cbl-interacting protein, is a component of AMAP1-mediated breast cancer invasion machinery. The EMBO journal 26: 647-656

72 Onodera Y, Nam JM (2007) [Breast neoplasms: invasion and metastasis]. Nihon rinsho Japanese journal of clinical medicine 65 Suppl 6: 33-38

73 Samoylenko A, Dimova EY, Kozlova N, Drobot L, Kietzmann T (2010) The adaptor protein Ruk/CIN85 activates plasminogen activator inhibitor-1 (PAI-1) expression via hypoxia-inducible factor-1alpha. Thrombosis and haemostasis 103: 901-909

74 Ma Y, Ye F, Xie X, Zhou C, Lu W (2011) Significance of PTPRZ1 and CIN85 expression in cervical carcinoma. Archives of gynecology and obstetrics 284: 699-704

75 Kim Y, Roh S, Park JY, Kim Y, Cho DH, Kim JC (2009) Differential expression of the LOX family genes in human colorectal adenocarcinomas. Oncology reports 22: 799-804

76 Kirschmann DA, Seftor EA, Fong SF, Nieva DR, Sullivan CM, Edwards EM, Sommer P, Csiszar K, Hendrix MJ (2002) A molecular role for lysyl oxidase in breast cancer invasion. Cancer research 62: 4478-4483

77 Chitu V, Pixley FJ, Macaluso F, Larson DR, Condeelis J, Yeung YG, Stanley ER (2005) The PCH family member MAYP/PSTPIP2 directly regulates F-actin bundling and enhances filopodia formation and motility in macrophages. Molecular biology of the cell 16: 2947-2959

Table S2. Genes enriched in Rac1high population and encoding transcription factors.

Ensembl gene ID	Symbol	Rac1 experiments				Cdc42 experiments	
		RNA-Seq*		qPCR	average FPKM	RNA-Seq*	qPCR
		Exp.1	Exp.2			Exp.1	
ENSRNOG00000012262	Depdc7	1.51	1.88	1.18	33.57	1.15	N.A.**
ENSRNOG00000001314	Fam20c	1.35	1.84	1.19	16.25	0.88	N.A.
ENSRNOG00000019965	Tgfb1i1	1.61	2.04	1.03	12.96	0.85	N.A.
ENSRNOG00000000640	Egr2	1.35	2.41	3.28	6.00	3.98	5.35
ENSRNOG00000018841	Sox8	1.54	5.20	N.A.	1.52	1.61	N.A.
ENSRNOG00000004109	Zfpm2	3.63	4.99	N.A.	1.24	1.14	N.A.
ENSRNOG00000028648	Olig1	2.77	7.76	N.A.	1.07	N.A.	N.A.
ENSRNOG00000008826	Pax9	2.02	2.35	N.A.	0.95	1.42	N.A.

*RNA-Seq was performed twice. Fold increase of $Rac1^{high}$ vs $Rac1^{low}$, or $Cdc42^{high}$ vs $Cdc42^{low}$ cell populations is shown.
**N.A.; not analyzed.

Table S3. Genes enriched in Rac1high population and encoding Rac1 activators

Ensembl gene ID	Symbol	Rac1 experiments				Cdc42 experiments		
		WAD rank	Exp.1	Exp.2	qPCR	WAD rank	Exp.1	qPCR
ENSRNOG00000018726	Elmo1	435	2.95	3.60	3.89	766	2.57	3.84
ENSRNOG00000016479	Plekhg4	504	0.71	0.55	0.60	9716	1.03	
ENSRNOG00000006952	Prex1	541	1.43	1.69	2.05	481	1.84	
ENSRNOG00000016728	LOC100362710	1103	0.69	0.52		6064	0.84	
ENSRNOG00000015026	ARHGB_RAT	1199	0.71	0.71		11806	1.00	
ENSRNOG00000023313	Arhgef19	1428	1.50	1.25		5272	1.12	
ENSRNOG00000001818	FGD4_RAT	1573	1.60	1.94		1197	2.47	
ENSRNOG00000020130	Arhgef1	1633	1.12	1.33		2366	1.16	
ENSRNOG00000004823	F1LUN1_RAT	1717	0.73	0.50		805	0.49	
ENSRNOG00000038970	Fgd1	1810	0.79	0.74		10120	0.98	
ENSRNOG00000017765	Net1	2280	0.72	0.79		6736	1.13	
ENSRNOG00000030266	Plekhg2	2391	1.38	1.43		4992	1.29	
ENSRNOG00000001304	Bcr	3026	0.85	0.76		10983	0.99	
ENSRNOG00000007733	Arhgef9	3154	3.67	6.11		260	2.98	
ENSRNOG00000014576	F1M4N6_RAT	3308	0.82	0.42		20750	0.93	
ENSRNOG00000000869	Arhgef6	3356	0.87	0.86		5928	0.90	
ENSRNOG00000001706	Kalrn	3384	0.87	0.73		385	0.42	
ENSRNOG00000020027	Arhgef2	3517	0.95	0.83		8618	0.97	
ENSRNOG00000022216	Abr	4824	0.95	0.83		2853	0.85	
ENSRNOG00000018683	Dock1	4854	0.94	0.89		1667	1.21	
ENSRNOG00000009910	Swap70	4941	1.21	1.02		10349	1.01	
ENSRNOG00000011203	Farp1	5098	1.00	1.17		6749	1.05	
ENSRNOG00000020485	Vav3	5141	1.57	1.09		3525	1.48	
ENSRNOG00000021569	D3ZTB8_RAT	5544	0.71	0.97		9806	0.97	
ENSRNOG00000012934	Arhgef7	6377	1.01	0.83		6127	1.09	
ENSRNOG00000007422	Vav2	6877	1.09	1.10		8559	0.95	
ENSRNOG00000024703	F1MA88_RAT	6881	1.03	0.83		5190	0.91	
ENSRNOG00000010964	Akap13	7218	1.09	1.04		2941	1.14	
ENSRNOG00000015894	Dock8	7232	1.01	0.81		1872	0.65	
ENSRNOG00000028426	Mcf2l	8326	1.00	0.75		2647	0.61	
ENSRNOG00000006570	Plekhg3	8421	0.92	0.95		8574	0.95	
ENSRNOG00000013321	Dock11	8933	1.89	2.78		20750	0.00	
ENSRNOG00000006701	Fgd6	9043	0.91	0.69		11143	1.08	
ENSRNOG00000005506	Arhgef5	9777	1.13	0.71		1085	0.48	
ENSRNOG00000011969	Dock9	9856	0.99	0.91		6614	0.90	
ENSRNOG00000004826	Sos2	9910	1.05	1.02		4542	1.15	
ENSRNOG00000023280	Als2	9935	0.97	1.10		5808	1.11	
ENSRNOG00000028090	Arhgef18	10122	1.02	0.92		5425	0.89	
ENSRNOG00000008924	Arhgef12	10923	1.13	0.92		6075	1.07	
ENSRNOG00000016011	Plekhg1	11624	1.03	1.01		11069	1.02	
ENSRNOG00000002001	Itsn1	11680	0.96	1.02		10061	0.98	
ENSRNOG00000018051	Farp2	11899	1.13	0.92		8672	0.93	
ENSRNOG00000016544	Rgnef	12021	0.95	1.02		5957	0.71	
ENSRNOG00000013707	Spata13	12168	1.01	0.97		961	2.32	
ENSRNOG00000010652	Dock6	12180	0.70	0.59		11040	0.88	
ENSRNOG00000014549	Sgef	12550	1.17	0.86		20750	1.68	
ENSRNOG00000000502	Def6	15330	0.00	0.00		20750	0.00	
ENSRNOG00000000528	Fgd2	15330	0.00	0.00		20750	0.00	
ENSRNOG00000003435	Mcf2	15330	0.00	1.83		20750	0.00	
ENSRNOG00000004566	Arhgef15	15330	0.00	2.75		20750	0.00	
ENSRNOG00000010213	F1LTE6_RAT	15330	0.00	0.00		20750	0.00	
ENSRNOG00000014025	Rasgrf1	15330	0.00	0.92		20750	1.35	
ENSRNOG00000014035	Arhgef4	15330	0.82	0.31		20750	0.00	
ENSRNOG00000014363	Arhgef3	15330	1.12	0.99		20750	0.13	
ENSRNOG00000016225	Fgd3	15330	0.17	1.53		20750	3.77	
ENSRNOG00000016653	Ngef	15330	1.03	0.92		20750	0.38	

*RNA-Seq of Rac1 was performed twice. Fold increase of $Rac1^{high}$ vs $Rac1^{low}$, or $Cdc42^{high}$ vs $Cdc42^{low}$ cell populations is shown.

Table S4. Primer sequences used for qPCR.

Adfp-Forward	tatgcctgcaaggggcta	Adfp-Reverse	gggcattggcaacaatct
Cdh13-Forward	caacccacagaccaacgag	Cdh13-Reverse	cagggtgtgaaaggcagag
Csgalnact1-Forward	ccggtcagacttcatcaaca	Csgalnact1-Reverse	ggagatatttccggtacaggtg
Ctsl1-Forward	ttgtgtgactcctgtgaagaatc	Ctsl1-Reverse	ccttctaggcaacccgatg
Depdc7-Forward	ctcccctcacgtctctacca	Depdc7-Reverse	gtccaatcgtctcctcttgc
Ecop-Forward	gccgttcctatgaagactgc	Ecop-Reverse	gccgttcctatgaagactgc
Egr2-Forward	ctacccggtggaagacctc	Egr2-Reverse	tctctccggtcatgtcaatg
Elmo1-Forward	cactattcttcgattaaccacgtc	Elmo1-Reverse	ttgatgactgtattcgttcatgg
Fam20c-Forward	gaggcacaatgcggagatag	Fam20c-Reverse	gaggcactctgcggaaatc
Fgfr3-Forward	ctcaggagatgacgaagatgg	Fgfr3-Reverse	cggtcgagtccagtaaggag
Freq-Forward	cctggatgagaagttgaggtg	Freq-Reverse	ccactatgtccagcatctcg
Hbegf-Forward	tgaccacactaccgtcttgg	Hbegf-Reverse	cataacctcctcgcctatgg
Il1rap-Forward	aagcagccaaggtgaaacag	Il1rap-Reverse	ctccagccagtaaacgtggt
Lgals3-Forward	aagcccaacgcaaacagtat	Lgals3-Reverse	tcattgaagcgggggtta
Loxl3-Forward	ccggtttctcagactccaac	Loxl3-Reverse	ctggtcggagtcgcactt
Maged1-Forward	caagagctatggctcagaaacc	Maged1-Reverse	agcaaggcgctgtcttctac
Mmp15-Forward	gaagacgccgaagtatacgc	Mmp15-Reverse	gctggggtaggtagccataga
Nid67-Forward	tcgcttgaggatcccttg	Nid67-Reverse	gctgatagcatccatgttgg
Ntrk2-Forward	accaatcgggagcatctct	Ntrk2-Reverse	gccaacttgagcagaagca
Prex1-Forward	ccatcaggaccctggtagac	Prex1-Reverse	gcagctggttcttcccatc
Prlhr-Forward	ggcgcatttcactgaagc	Prlhr-Reverse	cgccagcactgcagatag
Pstpip2-Forward	gctgcagcggaaaaagac	Pstpip2-Reverse	tgcgagttcctctgtttgtg
Rgs2-Forward	aacttttatcaagccttctcctga	Rgs2-Reverse	acgctctgaatgcagcaag
Sdc2-Forward	ttgatggcctgtgtgtcg	Sdc2-Reverse	ggagctgctgtcaaggtaca
Sh3kbp1-Forward	gaggaacacatttcgcttgc	Sh3kbp1-Reverse	gggaagccttgttatcagaca
Slc1a1-Forward	ttcctgcggaatcactgg	Slc1a1-Reverse	accaagactcctaccacgatg
Tgfb1i1-Forward	aacctattgctgggcaagtg	Tgfb1i1-Reverse	aacctctgcaaaggaagtgc
Tmem100-Forward	ggtccttctctcccaagtca	Tmem100-Reverse	aggttcagaaagcctgacca
Tsn17-Forward	gcccttctcctgctgtgtta	Tsn17-Reverse	tttggtgtagatggagccttg

Table S5. siRNA Sequences

Ap1s2-1	GAAUGAAAGUUUAUUGAAATT	Itgb3-1	GCUUUGACGCCAUCAUGCATT
Ap1s2-2	CUGAUUACCCUGGAAAUAATT	Itgb3-2	CAAGCAAUGUCCUUCAGCUTT
Ap1s2-3	GUGAAACCUGGUUUAAUGATT	Itgb3-3	CCAUGUUUGGCUACAAACATT
Cdh13-1	CUAUCAGGUACUCUGUUUATT	Lgals3-1	CACAGUGAAGCCCAACGCATT
Cdh13-2	CUUAUCAACUGUUUGUGGATT	Lgals3-2	CGGUCAAUGAUGUUCAUCUTT
Cdh13-3	CUAUGAGGUCUCAAGCCCATT	Lgals3-3	CCAACUGGCCCUAGUGCUUTT
Csgalnac-1	CCAUAAGCAUGAAUUCCAATT	MMP15-1	UCUCCAGCACUGACCUGCAUGGAAU
Csgalnac-2	GAUUUGACCUGGACAUCAATT	MMP15-2	GGACACCCAUUUCGACGCACAUGAA
Csgalnac-3	CAUAGCAACCUCAUAGUGATT	MMP15-3	ACAGAGAAGCUGGGCUGGUACAACU
Egr2-1	GUGACUAUUGUGGCCGUAATT	Ntrk2-1	GACAUCAUGUGGCUCAAGATT
Egr2-2	GUUUGACUAUGGUCUGCGATT	Ntrk2-2	CAAUGAAGAUGAUGUCGAATT
Egr2-3	GAAAGGAAGCGCCACACCATT	Ntrk2-3	CAAACAACGAGGUGAUAGATT
Elmo1-1	GUUUAUGACUGUAACUGAATT	Pstpip2-1	GAAAGAAAGGGCAUCAAUUTT
Elmo1-2	GCAUUUCACUCCUCACUCATT	Pstpip2-2	CCAUCAUGUAUGAGAAUUUTT
Elmo1-3	GGAUGAACCAGGAAGAUUUTT	Pstpip2-3	GUGAAACUGGCCACUUCGATT
Fbxo23-1	CGCCAUUGCCUCCUUCAAATT	Rgs2-1	GGUUGGCUUGCGAAGACUUTT
Fbxo23-2	GGCUAUACAUCCGCUCAAATT	Rgs2-2	GAGAUAAACAUAGACUUUCTT
Fbxo23-3	CCCAAUGACUGGAACCUCATT	Rgs2-3	CUUGCUGCAUUCAGAGCGUTT
Fgfr3-1	CACAUGACCUGUACAUGAUTT	Sdc2-1	CUUUAGCAUAGAAUAAUGATT
Fgfr3-2	GAGUCUAAUUCCUCUAUGATT	Sdc2-2	CAGUGUUCUGUGAAUAGCATT
Fgfr3-3	GCAUUAAGCUCCGGCACCATT	Sdc2-3	CUGACAACAUCCCAACUGATT
Freq-1	CACCAAGUUCGCCACGUUUTT	Slc1a1-1	CAGAUUCUGGUGGAUUUCUTT
Freq-2	GAACGCUGAUGGGAAGCUATT	Slc1a1-2	CCACAAUCCUGGAUAAUGATT
Freq-3	CGAAUUCAUCCAGGCUCUATT	Slc1a1-3	GGUAUUGUGUUAGUUGUGATT
Il1rap-1	GACUUACUGCAGCAAAGUUTT	Tmem100-1	GAUAUGCACAGCAUUAAAUTT
Il1rap-2	GGUUGUACUGAAAUAGUGATT	Tmem100-2	CAAAUAAUGGACAGGAUGATT
Il1rap-3	CUCAUAUCUACUCGCCAAATT	Tmem100-3	GGGAAUAACUCAUCUUCUUTT